2018-01-01

Design And Simulation Of Mems Actuators To Study Strain Behavior Of 2d Materials

Mariana Martinez
University of Texas at El Paso, harajukulovr94@yahoo.com

DESIGN AND SIMULATION OF MEMS ACTUATORS TO STUDY STRAIN BEHAVIOR OF 2D MATERIALS

MARIANA MARTINEZ

Master's Program in Electrical Engineering

APPROVED:

David Zubia, Ph.D., Chair

Jose Mireles Jr., Ph.D., Co-Chair

Sergio F. Almeida, Ph.D.

David A. Roberson, Ph.D.

Charles Ambler, Ph.D.
Dean of the Graduate School

Dedication

To my family, friends, and anyone who made my days just a little brighter

DESIGN AND SIMULATION OF MEMS ACTUATORS TO STUDY STRAIN BEHAVIOR OF 2D MATERIALS

by

MARIANA MARTINEZ, B.S.

THESIS

Presented to the Faculty of the Graduate School of

The University of Texas at El Paso

in Partial Fulfillment

of the Requirements

for the Degree of

MASTER OF SCIENCE

Department of Electrical and Computer Engineering

THE UNIVERSITY OF TEXAS AT EL PASO

August 2018

Acknowledgements

First I would like to thank my advisor, Professor David Zubia, for his guidance, support, and kindness in the years leading up to and during the writing of this thesis. I would also like to thank my other committee members, Professor Jose Mireles for his knowledge and guidance in all things MEMS as well as for his sense of humor, Dr. Sergio Almeida for his knowledge, guidance, and patience, and finally to Dr. David Roberson who was supportive and generous throughout the process.

To all the members of the NanoMIL group as well as to those I have met through E3S, I am incredibly grateful to have met such generous, humble, and intelligent individuals. Especially I would like to thank, Aldo Vidaña, Edgar Acosta, Dr. Rodolfo Aguirre, Dr. Sergio Almeida, and Dr. Arka Talukdar. This experience would not have been the same without your knowledge, support, and most importantly, friendship. I also wish to express my utmost gratitude to the faculty and staff UTEP's ECE department, as well as to the students, faculty, and staff of the E3S center.

Finalmente, agradecer a mi familia, palabras no bastan para expresar lo bendecida que he sido de tener su apoyo y amor incondicional. Especialmente a mi madre, por los sacrificios, amor, y dedicacion; simplemente no hay palabras, no soy nada sin ti mamá.

Abstract

Since the 60s the semiconductor industry has successfully been able to keep pace with Moore's Law due to the effective scaling of the silicon-based transistor. However, as scaling technology improves, passive power density has begun to dominate the overall power consumption of transistors. The inability to scale power density alongside the decreasing transistor dimensions has hindered the efficiency trend observed in the last decades. Thus, new alternatives have been researched to overcome the current power crisis. Micro-electro-mechanical system (MEMS) actuators offer excellent on/off ratios with very steep transitions. Furthermore, two-dimensional transition-metal dichalcogenide (TMD) materials have been studied due to their intrinsic properties, such as their relatively high strength and tunable bandgap resulting from mechanical strain. Semiconducting TMDs can switch between semiconducting to metallic state based on the uniaxial tensile strain they are subjected to. Furthermore, devices which exploit the bandgap tunability of the TMDs to enhance their conductivity have not been thoroughly explored. In this thesis, MEMS comb actuators were designed and simulated to achieve high electrostatic forces to mechanically strain the considerably stiff TMDs.

Comb-drive actuators were successfully designed for SOI and SiGe MEMS processes. A strain of 6% is predicted in the MoS_2 bilayer at sub-100 Volt operation for both cases. The SOI process has the advantage of a simpler fabrication process and greater stability due to the thicker device layer. On the other hand, the SiGe process has the potential for lower voltage actuation in the vertical direction due to a much thinner oxide layer.

Table of Contents

List of Tables

List of Figures

List of Formulas

Chapter 1: Introduction & Motivation

1.1 Limitations of CMOS

The complexity of our ever-evolving electronic devices has been made possible in great part by the semiconductor industry which has preserved a scaling trend of Complementary Metal Oxide Semiconductors (CMOS) transistors to follow Moore's Law. Transistors are the foundation of the integrated circuits and therefore all electronics, in 1965, their minimum feature size was 50um, totaling about 50 components per chip. [1] Doubling the number of transistors per chip every two years has allowed current minimum feature size to be in the nanometer range and the transistor count to be in the billions. [1] Materializing Moore's law as a result of design (i.e. dimension miniaturization) and evolution of fabrication capabilities has enabled the advancements observed in performance and functionality while continuously lowering costs.

The success in following Moore's Law has allowed technology to flourish and reshape the landscape of our society. Enhancements in performance at lower costs has facilitated advancements in various technological sectors, such as mobile internet, cloud computing and data analytics. [2] In turn the advancements in these technologies has greatly accelerated the demand and proliferation of electronics in society for a wide variety of applications.

However, while the complexity and sophistication of electronics has grown at unprecedented rates due to incessant miniaturization of transistor dimensions, the power consumed by the MOS transistors have no longer scaled since the turn of the century. Augmenting power consumption, due mainly to static power dissipation has continued to increase as the dimensions of devices have been reduced. This poses a serious energy consumption problem as the proliferation of electronics continues.

The rise of cryptocurrencies, such as Bitcoin, is a prime example of how the use of modern electronic technologies are creating a power consumption problem. Cryptocurrency is electronic or virtual money. Unlike physical currency which requires banks, or a middle man in order to execute transactions, virtual money is decentralized and does not require third parties in order to carry out a secure transaction. [3] The backbone of cryptocurrencies is Blockchain technology which is essentially a public electronic ledger that is open for anyone in the world to see and change. [4] The way cryptocurrencies use Blockchain technology is by creating records of each transaction in the open ledger. A "block" is a record of various transactions which contains the necessary information concerning the exchange and overall business activity. Upon the creation of the block, it is made public to all the computers on the network. Once a block is created it is linked to previous transactions, therefore blocks thus creating a "block-chain". [5] Although seeing the information stored in the block-chain is easy, creating a block that includes the information of various transactions can be computationally costly. The computers in the bitcoin network are referred to as nodes, some of which are "miners", meaning they are responsible for the verification of transactions in order to create blocks. The creation of blocks requires substantial computational resources due to the straining amount of calculation required for their creation. [5]. A major cost to miners is the electricity consumed by their computers, this is due to the hefty computational resources needed to create and authenticate the information of new blocks. The time and power required to create and verify information pertaining to each transaction will continue to rise as a result of the increasing number of users, and therefore rising business activity. While global use of cryptocurrencies may still be in its infancy stages, the power consumed currently is already greater than certain small countries, according to estimates from Digiconomist, as illustrated in Figure 1. Figure 1 shows that the power consumed by Bitcoin already surpasses that of the Czech

Republic. This is just one example that showcases the need for greater efficiency in electronics is fundamental to the evolution of technology.

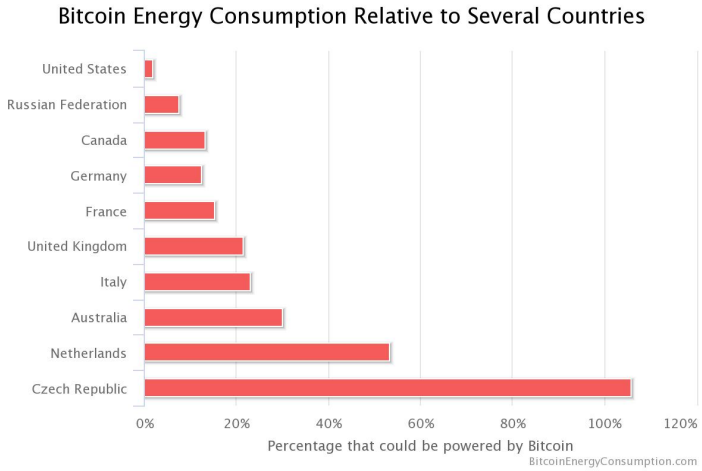

Figure 1: Bitcoin's energy consumption

The increase in static power dissipation is a major limitation to further miniaturization of CMOS. In the subthreshold region of operation, the minimum subthreshold swing (which is expressed as the applied voltage needed for a decade increase in output current) theoretically limited to 60mV/dec (due to the thermal voltage). [6] The fixed subthreshold swing is a fundamental limit in the transistor, while the off-state current (I_{off}) is proportional to $10^{\frac{-V_t}{ss}}$. [6] The scaling of the threshold voltage has a detrimental effect to the static power consumption of the device due to the exponential rise it has on the off-state currents, therefore setting a limit to which the threshold voltage can realistically and advantageously be reduced to. Furthermore, the lowering of supply voltage (V_{dd}) poses its own issues in preserving performance and must be scaled cautiously. Augmenting performance comes at the cost of energy efficiency or boosting efficiency degrades performance. [7] As a result, maintaining a scaling trend that increases speed and transistor density while reducing power consumption has become a challenging problem in the last years. [8]

Based on the effects that derive from the miniaturization of CMOS such as the aggravation of the off-state power dissipation, energy efficiency must be sought in a new low voltage switching device in order to elude the power crisis we currently reside in.

1.2 STRITCH DEVICE

To address the energy inefficiency of MOS transistors and reliability problems with mechanical relays a new device called the "Stritch" was recently proposed. [9] The Stritch device integrates MEMS actuator with a thin (2-dimensional) material to create an energy efficient electro-mechanical switch. The device offers characteristics which overcome certain plaguing characteristics of both electronic silicon-based transistors as well as mechanical relays. These include; <60 mV/dec subthreshold swing, a current on/off ratio of 10^6, and the elimination of failure due to adhesion between mechanical components of the relay (stiction, which can be detrimental to the reliability of MEMS). [10] Importantly, the Stritch device also has the potential of being 10 times more energy efficient compared to the MOS transistors.

The proposed device (illustrated in Figure 2) uses a MEMS actuator to strain a thin transition-metal dichalcogenide (TMD) layer. TMDs have interesting properties such as their change in conductivity, which increases exponentially when they are strained. (This property is called deformation potential.) Thus, when the TMD is strained by the MEMS, its conductivity changes exponentially causing it to function like a switch.

Bilayer of molybdenum disulfide (2L-MoS_2) was selected for the TMD material due to its high deformation potential. Additionally, having even number of layers is important to avoid piezoelectric effects present in odd number of layers. [11] The TMD is clamped between a cantilever (source) and a contact pad (drain) as shown in Figure 2. Upon application of a voltage between the gate and source (V_{GS}), an electrostatic force displaces the cantilever towards the gate,

therefore mechanically straining the TMD. [10] The mechanical strain of the TMD causes an exponential increase in its conductivity. [10] The bilayer TMD will become metallic at 6% strain. [12] For 2L- MoS_2 the calculated strain needed to achieve an increase in conductivity of 10^6 is 6%. The focus of this thesis was to design a MEMS actuator which will strain the TMD to a critical strain of 6%.

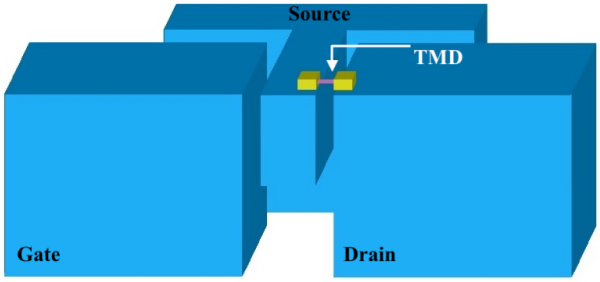

Figure 2: Stritch device

1.3 CONTRIBUTIONS OF THIS THESIS

The contribution of this thesis is the design of a MEMS actuator for the Stritch device, which is al low power alternative to the transistor. The Stritch device is a switch which employs MEMS actuators and the bandgap deformation of two-dimensional materials in order to alternate between off and on states. [9] Analytical and simulated analyses of the design are investigated in order to predict device performance. Various manufacturing and operational constraints are taken into consideration to arrive at a satisfactory solution.

Chapter 2: Technical Background

2.1 Transition Metal Dichalcogenides (TMDs)

Silicon has been the reigning material in semiconductors since the 60s. While other materials may have better properties, the shortcomings of silicon have been mitigated by its abundance (i.e., low-cost), excellent oxide, and advanced technology (i.e. doping). [13] However, silicon-based transistors are reaching a fundamental scaling limit due to current leakage and increasing power dissipation. Because of this, alternative materials have been explored to counteract the deficiencies of silicon.

While the isolation of the first two-dimensional material, graphene by Andre Geim and Kostya Novoselov in 2004 may be have been by chance, it shook the science community due to its compelling properties which are diametrically opposed to its bulk form. [14] Graphene has strength, flexibility, and electronic properties unlike any other material. [15] While the properties of Graphene were phenomenal, it lacked a bandgap. Considering the semiconductor applications in which the bandgap allows the transition between on and off state, the lack of it thwarted the use of Graphene as a switching device.

In order for a material to even begin to compete with silicon, it must have a bandgap, and while graphene does not naturally have one, its extraordinary properties encouraged the search for other two-dimensional materials with semiconductor characteristics. A group of 2D materials of which many are semiconducting, are referred to as transition metal dichalcogenides or TMDs. The structure TMDs (chemical formula, MX2) consist of a transition metal atom (M), sandwiched between two chalcogen atoms (X2). Chalcogens include sulfur, selenium, and tellurium as illustrated in Figure 3. Particular interest lies in the TMDs with molybdenum (Mo) due to its

semiconducting nature, enabling it to become viable alternatives in electronic switching applications. [16]

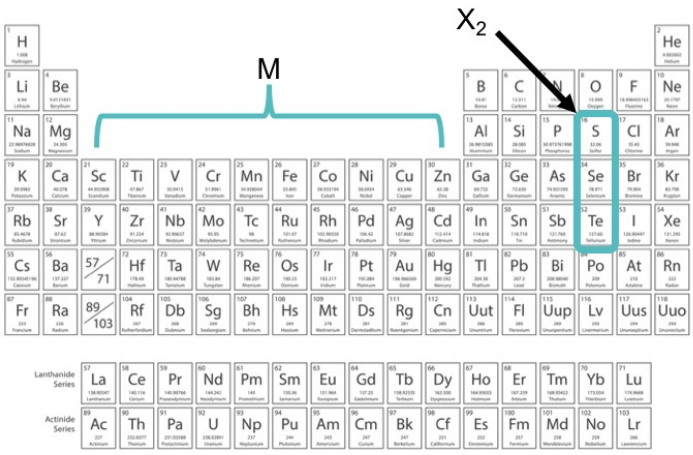

Figure 3: TMDs on Periodic Table [17]

2.1.1 2D Semiconducting Materials: MoS_2

MoS_2 consists on a Molybdenum atom (M) sandwiched between two Sulfur atoms (X2) in a honeycomb crystal lattice. Due to the weak Van der Waals forces joining the many layers of the material, MoS_2 can be isolated into a stable monolayer similar to other 2D materials. [16] Of the possible combinations of TMDs, MoS_2 is one of the most studied due to its interesting semiconducting properties, such as tunable bandgap, high on/off current ratio, and mobility.

Notably, MoS_2 has interesting mechanical and electronic properties such as high stiffness and a changing band structure resulting from thickness alteration and mechanical strain. MoS_2 like graphene has demonstrated to be a very strong material. Bertolazzi et al. obtained experimental data that established that in plane stiffness of a single layer of MoS_2 is ~180 ± 60 Nm^{-1}, while it has a Young's Modulus that may surpass that of steel (~200GPa), being ~200 ± 60GPa for bilayer. [18] The fracture point for MoS_2 as a result of strain can be as high as 11%, compared to that of silicon which is 0.7%. [11] Furthermore, MoS_2 possesses a tunable bandgap as a function of

mechanical strain. Its electrical properties can be tuned as a result from mechanical strain without rupturing the material based on the 11% level of strain it can undertake without fracture. The transition between semiconducting to metallic is reached at 6% tensile stain for 2L-MoS_2 respectively according to Kis et al. [12].

2.1.2 Exfoliation of TMDs

The strong in-plane bond and weak van der Waals forces holding the multiple atomically thin films of MoS_2 in bulk form allow for effortless isolation of individual layers. [19] The method used to obtain flakes of varying layer thicknesses is the exfoliation or mechanical cleavage/scotch tape method, originally used to obtain the first samples of 2D graphene. [20] The method is illustrated below in Figure 4, and is accomplished as follows: A piece of scotch tape is placed across a crystal source of MoS_2, upon the removal of the tape from the crystal, flakes of varying thicknesses have remained on the tape. This tape is placed on top of a Si-SiO_2 wafer with a silicon dioxide thickness of ~270nm. The thickness is important because it is a simple method used to estimate the thickness of flakes. The color contrast between the flake in comparison to the oxide allows for a primary assessment of flake thickness. [18] Upon the removal of the tape from the wafer, various flakes of material of varying number of layers remain on the wafer. From experimental work, a standard color scheme has been devised for easy identification of mono, bi, tri layer or bulk thickness of various 2D materials, therefore based on the color of a flake an initial assumption can be made.

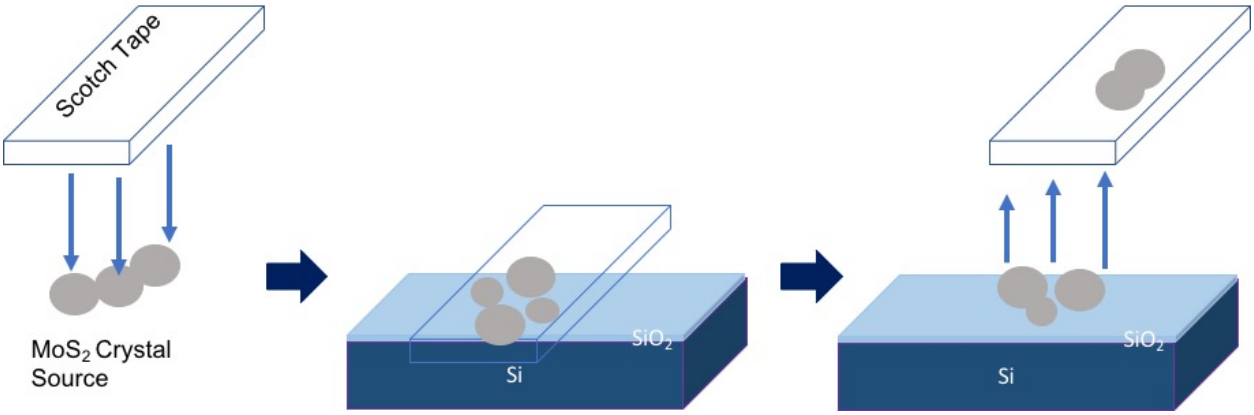

Figure 4: Exfoliation method of TMDs

2.1.3 Characterization

While a preliminary assessment of the flakes based on the optical contrast is used to predict their thickness such as mono or bilayer, their thickness must be confirmed by precise characterization methods such as Raman spectroscopy. Raman spectroscopy is a characterization method used to study the electronic band structure characteristics of a material. Here it is used to identify the thickness of a material based on specific Raman spectra which is unique for each material. [21] Upon the use of a 532nm laser for sample excitation, MoS_2 has two dominant peaks in its spectrum which correspond to the vibrational modes of E^1_{2g} (resulting from in-plane vibrations of S atoms with respect to Mo) and A_{1g} (resulting from out of plane vibrations of S atoms in opposing directions). [22] As illustrated in Figure 5, the peaks corresponding to the vibrational modes experience a shift, the resulting spectra is unique for the varying thicknesses of MoS_2 or other materials and is used as an established blueprint to identify the thickness of the sample based on the spectrum obtained. Other methods of characterization are also used such as Photoluminescence or Atomic Force Microscopy (AFM).

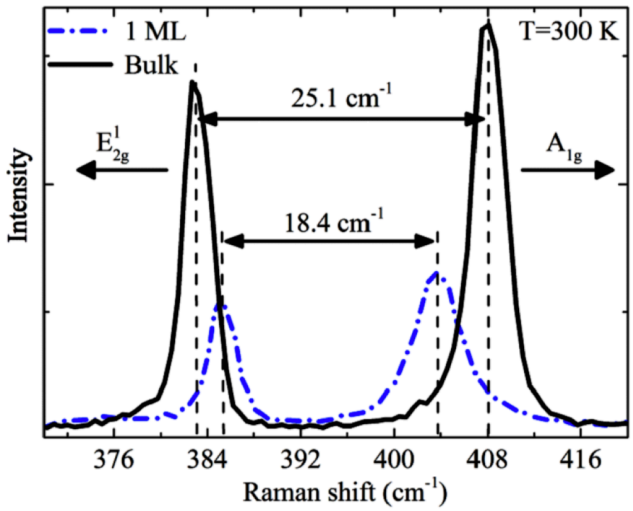

Figure 5: Raman Spectrum of MoS2 from bulk to monolayer [21]

2.2 Micro Electro Mechanical Relays (MEMS)

2.2.1 Background & Mode of Operation

Replaced in the early days due to their unreliability and slow speed in computing, the mechanical relay presents an ideal alternative to compensate for the weaknesses in the transistor. [23] The rising difficulty in miniaturizing the features of CMOS has led the static power consumption to escalate at alarming rates, thus leading to the resuscitation of past technologies in the quest for energy efficient alternatives.

Before the transistor, the foundation of the early computers was the relay, and later the vacuum tube, while they both presented deficiencies, the relay unlike its successors presented no idle power loss. [23] An electromechanical relay is a switch that opens and closes upon the contact, or lack thereof its mechanical components as the electrical signal is applied, as seen in Figure 6, which depicts a three terminal micro-electro-mechanical (MEM) cantilever switch.

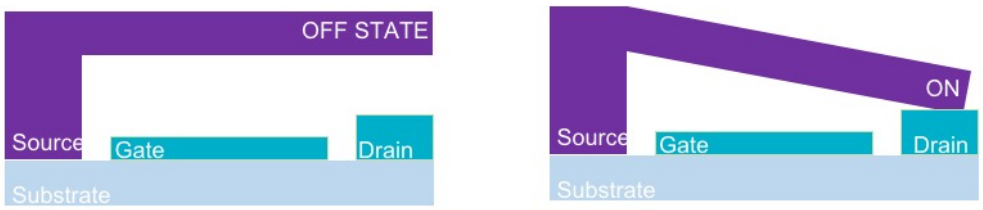

Figure 6: 3 Terminal MEM Switch

Using the same terminology as that of the MOSFET, the input voltage is applied to the "gate" terminal, upon the augmentation of the gate voltage, at a certain point, an equivalent of the threshold voltage, the pull-in voltage, "Vpi" will be reached. When this point is reached, the electrostatic force between the fixed "gate", and movable "source" terminal will be large enough to attract the movable source towards the "drain" terminal. [6] Given the physical structure of the relay, the on state is achieved once the contact between the terminals is established, and off state is achieved immediately upon the loss of aforementioned contact. The abrupt on/off switching of the relay due to the physical contact required to differentiate between on and off state allows ideally, for the equivalent of having a zero subthreshold swing (SS ~ 0) as seen below in Figure 7. The lack of dependence of I_{off} on the threshold voltage, allows for unrelenting scaling of V_{th} and therefore V_{dd}, lowering the overall power consumed by the devices without diminishing performance. [6]

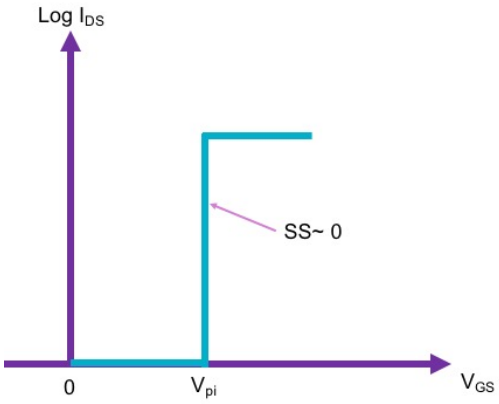

Figure 7: SS of MEM Relay

2.3 COVENTORWARE MEMS FEA SIMULATION TOOL

Coventorware is a finite element analysis (FEA) simulation tool which allows the design and simulation of MEMS. This simulation tool follows a realistic approach to the design and fabrication of MEMS. The process flow of the software is illustrated in Figure 8.

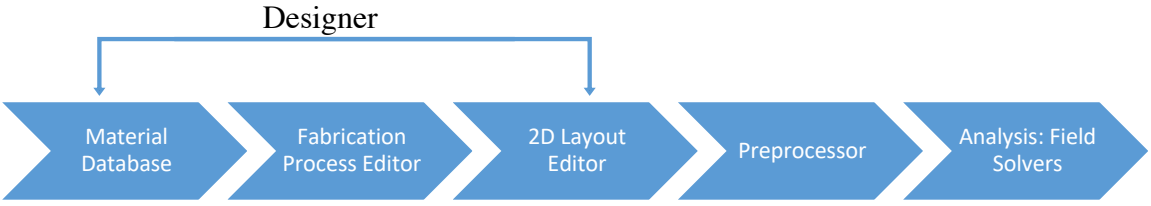

Figure 8: Coventorware process flow

2.3.1 Designer

As observed in the workflow of the design process (Figure 8), the design of a device is composed of various elements. These include a fabrication process with specific materials of unique characteristics, a schematic of the design, and finally the analysis. From this, it is understood that design begins with different materials of varying characteristics. The properties of the materials used in each process must be included in the materials database of the software,

which include the elastic constants (Young's Modulus, Poisson's Ratio), density, thermal conductivity, etc. Upon having the information of each material corresponding to their experimental or theoretical values, the process of fabrication is implemented in the process editor. While prototype processes are included, a custom fab process may be created, each step in the process may be defined as deposition, lithography (+/- photoresist), etching (wet, dry, DRIE, etc), with the corresponding values for thickness, material, and etching depth. For a more realistic approach, other parameters can be included, such as sidewall angles resulting from etching, mask offset, rounded corners, etc. After having specified the desired fabrication process in the process editor, the 2D layout editor is used to create the design for the corresponding masks utilized in fabrication for the desired device. In intricate or complex structures, the utilization of other layout tool editors is advised, such as L-Edit.

2.3.2 3D Model-Preprocessor

After determining the materials, fab process, and design layout of the device, the three-dimensional model is built in the preprocessor which is only one step away from the analysis of the device. Once the 3D model is loaded into the preprocessor, only the layers which are subject to analysis will be chosen to be meshed, those that do not contribute to the actuation mechanism go unmeshed. Before applying the overall mesh to the device however, areas of the device which are anchored, subject to applied voltage, or in general, regions which are exposed to higher degrees of scrutiny in the resulting analysis must be clearly identified. The method of doing this is by naming the corresponding areas of the device. Consequent to the identification of the critical regions of the device, the mesh is created. The mesh of the model is the deconstruction of the device into smaller elements of different shapes, there are various types of meshes which fit accordingly to different structures based on the geometry of the device such as hexahedrons or

tetrahedrons. [24] Depending on whether the chosen mesh is rough or refined, the results of the conducted simulation will show drastic differences and therefore accuracy. The selection of a mesh, such as Manhattan bricks, which is optimum for orthogonal geometries, divides the device into thousands of 'brick' elements, each element will have various nodes along the edges in which calculation is performed. Meshes are selected based on the geometry of the device, as well as on the computational resources available, due to the varying needs of computationally extensive meshes.

Upon the selection of the mesh type used, certain parameters of the mesh can define its quality; later to be supported by the comparison between analytical and simulated results. Once the mesh characteristics are chosen, such as the mesh type, and its element size, its quality is studied. A critical element to consider is the aspect ratio of which defines the quality of the elements of the mesh. The value of 1 is given for a perfect element, in the case of Manhattan bricks, a perfect brick, due to the ratio between the length of the box edges of the cube. The higher the aspect ratio value is, the poorer the shape of the element will become. The distortion of the elements reflects in the accuracy of the analysis, due to the calculation done at various nodes along the edges of the mesh, elements a high aspect ratio can lead to inaccurate results. The quality of the mesh is fundamental to obtain accurate results from analysis. The quality of the mesh can be observed in the "QualityQuery", where various characteristics of the mesh are given in order to determine whether it is ideal for the analysis conducted. Ultimately once an initial mesh is deemed fit, the device can be analyzed.

2.3.3 Field Solvers

The software allows various types of solvers, which allow the analysis of behavior such as electrostatics, mechanics, electromechanics, thermomechanics, and piezoelectrics. [24] The work

of this thesis will focus on the use of two solvers specifically, MemMech to simulate mechanical behavior, as well as the CoSolveEM to execute electromechanical analysis.

Chapter 3: Design Considerations and Approach

3.1 Design Considerations

The contributions of this thesis is the design of MEMS actuators applied to the fabrication of Stritch electro-mechanical switches. The design process must take into consideration various properties of the Stritch device, such as electrical and mechanical properties of the TMD and MEMS, as well as fabrication capabilities available; these are summarized in Figure 9 below.

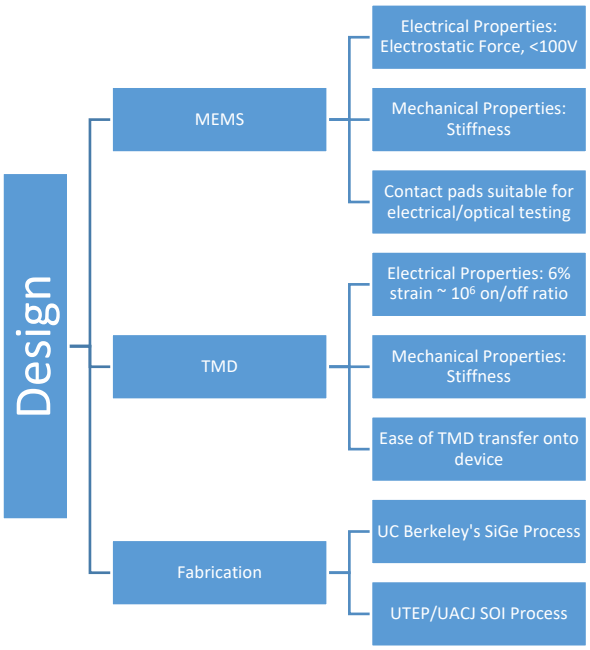

Figure 9: Design considerations and constraints

The main objective of the design is to achieve a compact device which could mechanically strain a TMD up to 6% at 100 volts or less. The less actuation voltage required in order to obtain the necessary percent strain, the better. In order to realize a device with all the necessary design characteristics, a force balance model was utilized to construct the analytical work. The force balance model encompasses three forces; the electrostatic force and the mechanical restoring

forces of the MEMS and TMD itself. The electrostatic force results from the geometry of the MEMS and the applied voltage. The mechanical restoring force of the MEMS results from the geometry and material properties of the MEMS springs. Lastly, the TMD restoring force results from the size and stiffness of the TMD material.

Although many types of MEMS actuators exist, a comb-drive actuator was chosen to achieve a <100-volt operation and smooth motion control. Comb drive electrostatic actuators are commonly used due to their fabrication and design simplicity. While a compromise must be made between impractically large areas or high operational voltages, overall, they grant stability and good sensitivity in actuation. [25] That is to say, a crucial tradeoff exists between high electrostatic force and area to prevent exceedingly large voltages, or device dimensions.

Limiting the length of the actuator's components reduces susceptibility to stresses in which movable components experience flexure even at zero applied voltage. However, the electrostatic force of the MEMS should still be sufficiently large to reach 6% TMD strain. It should be noted that TMDs have considerable stiffness based on their material properties, as a result the design should produce enough force and stability to strain the TMDs to 6%. This is accomplished by enhancing the force based on geometry and voltage, and device flexibility based on spring design. Spring choice determines the stiffness of the MEMS, therefore spring choice and compact size are important parameters to achieve good control of operation while reducing propensity for deflection in components.

Based on the crucial role played by the TMD in the overall operation of the device and its significant stiffness, an important manufacturability consideration is the transfer and clamping of the TMD onto the MEMS actuator. The design of the MEMS must facilitate the transfer and anchoring of the TMD. This requires the addition of pads where the TMD is anchored between the

actuating and fixed components. These pads also serve as contact pads for electrical and optical probing of the device. The number of pads must be limited to the minimum required for probing the three terminal device and should be sufficiently large (at least 100um x 100um) to allow wire bonding.

The fabrication process is crucial to the overall design due to the limitations they impose. In this thesis, the MEMS actuators were designed using two fabrication processes. One process is a standard silicon germanium (SiGe) process at UC Berkeley. The second process is a silicon on insulator (SOI) process jointly developed by UTEP and UACJ. Due to the different characteristics of the different processes, two comparable designs with different feature sizes and general tweaks are optimized to satisfy and take advantage of the limitations/capabilities set by the SOI and SiGe processes.

3.2 DESIGN APPROACH

Given the constraints, a method of execution to achieve a suitable design was devised. The point of commencement lies in the most basic form, which is the consideration of the force balance model, observed in Equation 1. The force model includes the governing forces of the actuator, the electrostatic force (F_E), mechanical restoring force of MEMS (F_{MEMS}), as well as of the TMD (F_{TMD}).

$$F_E = F_{MEMS} + F_{TMD}$$

Equation 1: Force Balance Model

Comprehension of the forces that act on the device are essential in order to model it analytically. Mechanical actuators are affected primarily by the electrostatic F_E, and the spring restoring force (F_{MEMS}), however the use of a TMD also significantly and predominantly affects

the design as shown in Figure 10. Thus, the forces affecting the MEMS must also include the effect of the force of the TMD (F_{TMD}).The TMD force is modeled as a spring using Hooke's Law as illustrated in Figure 10.

An important aspect of the design approach is the size (length, width, and thickness) of the TMD as the dimensions will determine the maximum TMD restoring force, F_{TMD}, at the critical strain. The sum of the TMD and MEMS forces can be used to estimate the maximum force needed by the actuator according to Equation 1.

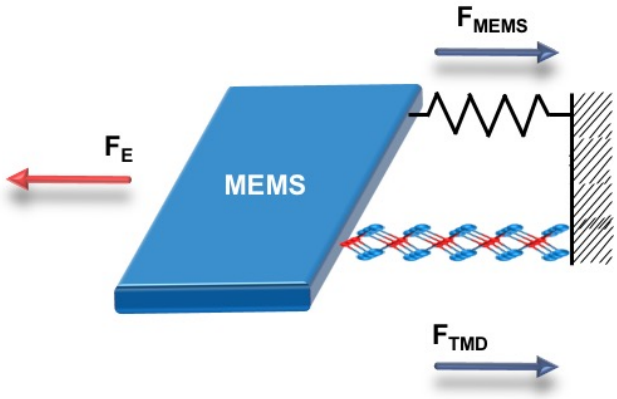

Figure 10:Force balance model

Chapter 4: General Analytical Model

4.1 Introduction

In the Stritch device proposed by Almeida et al. [10], a cantilever MEMS actuator was used to theoretically predict an on-off current ratio of six orders of magnitude (10^6) with an applied voltage of 75mV. These remarkable characteristics relied on a MEMS actuator with actuating gaps of 10nm which activated van der Waals forces that worked in unison with the electrostatic force to achieve the required cantilever displacement at very low operational voltage. However, in practice achieving such small actuating gaps is technically very challenging and beyond the capabilities of the SOI and SiGe processes. The actuation gaps achievable with SOI and SiGe processes are 1µm and 0.5 µm, respectively. Such large gaps will greatly diminish the electrostatic force of a cantilever actuator. In contrast, comb-drive actuators present various characteristics suitable to counteract the deficiencies present in the cantilever design. These include; greater control in the actuation and greater electrostatic force. Furthermore, comb-drives are commonly used due to their modeling and fabrication simplicity.

4.2 Comb-Drive Actuator

4.2.1 Electrostatic Force

As aforementioned, the electrostatic force of the cantilever is considerably less than that of the comb-drive actuator, this is due to the unfavorable effect caused by geometry. The electrostatic force of a cantilever is seen below,

$$F_{E\_Can} = \frac{\varepsilon_0 A V^2}{2g^2(1 - \epsilon)^2}$$

Equation 2: Cantilever Electrostatic Force [10]

where ε_0 is the permittivity of free space, A is the area of the device, V is the applied voltage, g is the actuation gap at zero voltage, and ϵ is the strain. In contrast, the electrostatic force of a comb-drive is given by,

$$F_{E\_Comb} = \frac{n\varepsilon_0 t V^2}{g}$$

Equation 3: Comb Drive Electrostatic Force [26]

where n is the number of finger pairs, t is the thickness of the device, V is the applied voltage, and g is the gap between the fingers. Analysis of Equation 2 of the cantilever shows that the force is proportional to the inverse square of the gap. As a result, the cantilever will only obtain considerable force from small gaps. In contrast, the force in the comb-drive is proportional to the inverse of the gap (Equation 3). However, in the comb-drive, the gap remains constant even during actuation and this creates a more consistent force. Additionally, the force of the comb-drive is proportional to the number of fingers which gives this design an added degree of design freedom to achieve the desired force. However, a trade-off in augmenting force by adding fingers lies in an increase in the size of the actuator. The design must then consider both size and voltage to find a balance in the design trade-offs made, in order to avoid an impractical design resulting from large area or voltage. The force balance model can be used to calculate the necessary electrostatic force which must be created to obtain the desired displacement by summing the restoring forces of the MEMS and TMD as given in Equation 1.

Figure 11 illustrates the comb-drive actuator. The structure of the comb-drive is formed by two interdigitated comb electrodes known as the stator and rotor. The stator is fixed while the rotor is suspended by springs to allow lateral motion. The application of ground to the rotor, and voltage

to the fixed stator creates a voltage difference between electrodes resulting in the creation of an electrostatic force that allows the movement of the rotor towards the stator. [27]

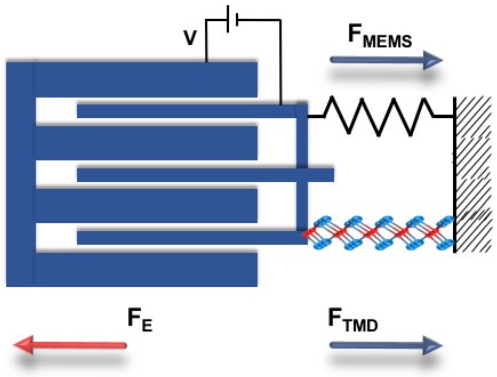

Figure 11 Comb drive actuator

The comb-drive in Figure 11 is subject to the MEMS and TMD spring restoring forces. The force balance model assumes the system is at static equilibrium and all the elements are considered to be massless. When the applied voltage is zero, all the forces are zero and the displacement is also zero. However, when the applied voltage is greater than zero, an electrostatic force is generated in the comb-drive that will pull the rotor towards the stator (to the left) as seen in Figure 11. However, this force is exactly balanced by the sum of the MEMS and TMD restoring forces created, due to the displacement of the rotor. In this way, the displacement increases with increasing voltage. This is the basic principle of actuation.

4.2 MEMS Force: F_{MEMS}

The stiffness of the device relies on the springs that suspend the movable rotor. The restoring force of the MEMS can therefore be modeled as a linear spring using Hooke's Law, as follows

$$F_{MEMS} = k_{MEMS}x = k_{MEMS}\, d\, \varepsilon$$

Equation 4: Comb Drive Mechanical Spring Force

where k_{MEMS} is the stiffness constant of the movable component due to the springs that suspend it, *d* is the gap where the TMD will be anchored (TMD gap), and ε is the strain. The TMD gap (*d*) is fixed during fabrication. However, the strain (ε) will vary from zero and upwards to the desired on/off ratio of 6% depending on how much voltage is applied. The remaining adjustable parameter is the stiffness constant (k_{MEMS}) which is obtained from the springs chosen for the design.

The spring constant of the MEMS is estimated by the elasticity of the springs used for the device. A smaller spring constant can allow for greater degrees of movement at lower voltages based on the materials and spring geometry. [28] There are various spring designs used for comb-drive actuators, however the design chosen for this device is the folded beam as shown in Figure 12. The folded beam is less prone to stresses due to the high stiffness ratio. This means that it has a different stiffness in the different axes, x, y, z, and commonly used in MEM actuators. [29] The stiffness in the y direction of motion is derived by modeling each of the 8 beams that make up the four folded beams. These beams are modeled as fixed-guided beams, fixed at one end and free at the other, where a load is applied, essentially Hooke's Law for a cantilever beam. After obtaining the stiffness for each beam, based on their series or parallel connection they are added and ultimately resulting in the equation given by

$$\mathrm{k_{MEMS}} = \mathrm{k_y} = \frac{2Ew^3t}{L^3}$$

Equation 5: Analytical Spring Constant of MEMS [29]

where *E* is the Young's Modulus of the material, *w* is the width, *t* is the thickness, and *L* is the length of the beam, shown in Figure 12.

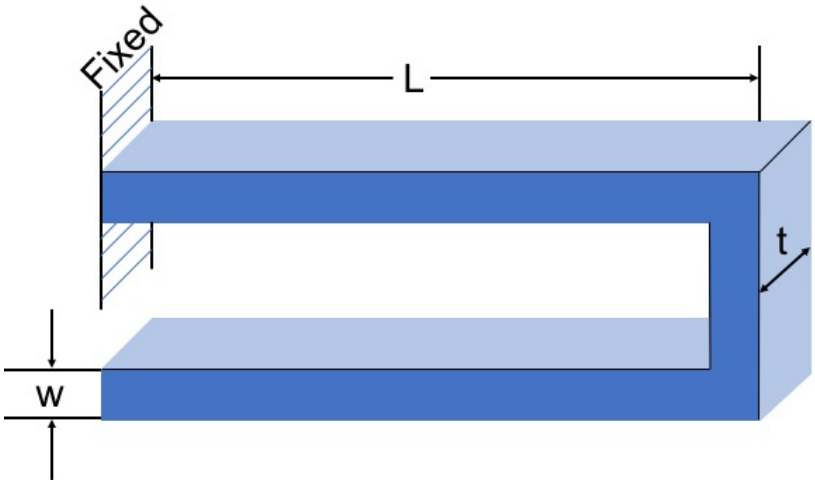

Figure 12: Folded Flexure Spring

The concept of Hooke's Law is also employed to obtain the mechanical restoring force of the TMD as follows,

$$F_{TMD} = k_{TMD}x = k_{TMD}\, w_{TMD}\, \varepsilon$$

Equation 6: TMD Mechanical Spring Force

where k_{TMD} is the stiffness constant of the TMD, w_{TMD} is the width of the TMD (in this thesis, the TMD is modeled to have a square geometry where the length is equal to the width to simplify the analysis, and allow for independence of the MEMS in analysis, it can be seen in Figure 13), and ε is strain.

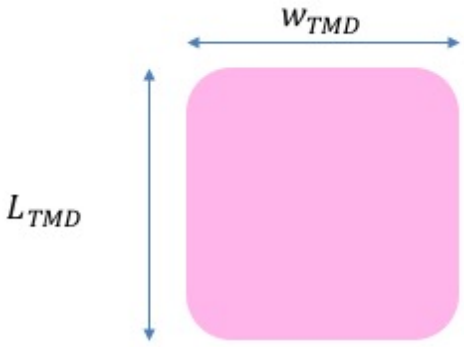

Figure 13: TMD

The stiffness constant of the TMD material is based on its intrinsic properties (Young's modulus) and physical size. Here a bilayer (2-layer) of MoS_2 was selected due to the piezoelectric effects observed in TMDs with an odd number of layers. [12] As mentioned previously, the geometry of the TMD is assumed to be a thin square membrane where t << $L_{TMD} = w_{TMD}$. Thus, the stiffness of the TMD can be modeled as the product of the Young's modulus and the thickness as follows:

$$k_{TMD} = \frac{E w_{TMD} t}{L_{TMD}} = Et$$

Equation 7: Stiffness of TMD

Where E is the Young's modulus, w_{TMD} is the width, L_{TMD} is the length, and t is the thickness of the material. A bilayer of MoS_2 has the Young's modulus of 140GPa and a thickness of 1.3nm (0.65nm per layer). [18] Therefore these parameters yield a k_{TMD} of 182 N/m.

4.3 Model and Architecture of Stritch Device

Now that the actuator, springs, and TMD were clearly defined in the previous sections, the force balance model can now be expressed using more fundamental material and geometric parameters as follows:

$$\frac{n\varepsilon_0 t V^2}{g} = k_{MEMS}\, d\, \varepsilon + k_{TMD}\, w_{TMD}\, \varepsilon$$

Equation 8: Force Balance Model of Comb Drive TMD Actuator

Certain parameters of the force equations are fixed due to material properties or fabrication. Therefore, the design must adapt and optimize based on the different SiGe or SOI processes. Furthermore, the comb-drive has various adjustable parameters in its geometry which affect its overall sensitivity to actuation. These parameters include, finger overlap, width, length, spring

width and length. These are chosen within the possible range based on the limitations of each fabrication process, and to optimize the device's operation. However, to give more definition to the design of the Stritch device, the general architecture is shown in Figure 14, which was created for the SOI and SiGe designs.

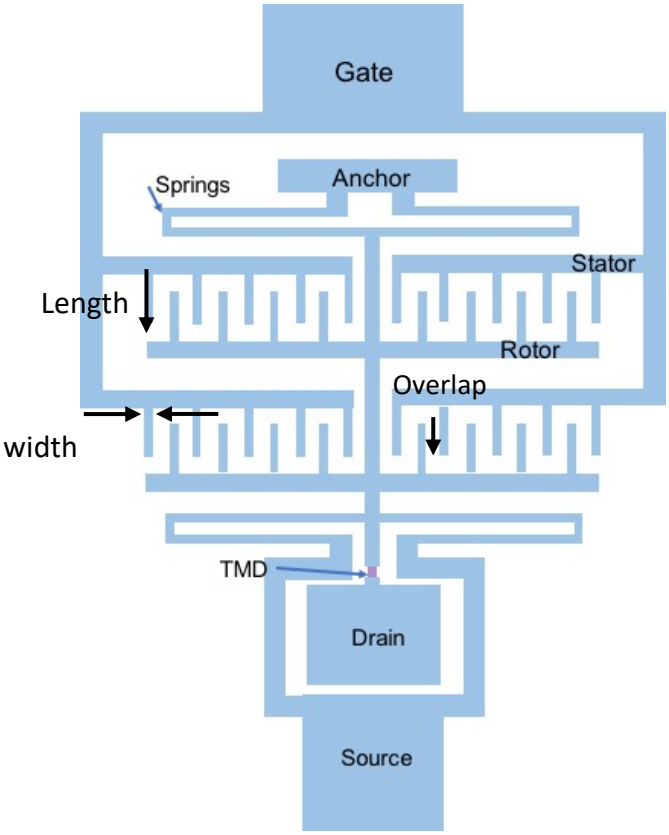

Figure 14: Comb drive device architecture

Chapter 5: SOI Design

5.1 Introduction

The processing of the SOI device is done collaboratively between UTEP and the Universidad Autonoma de Ciudad Juarez, consisting of a simple one mask process. The comprehension of this process is critical since device parameters are chosen based on materials and fabrication capabilities, therefore influencing the final device characteristics. The goal to the device is to adapt to each process and ultimately achieve 6% TMD strain with operational voltage below 100 volts.

5.2 SOI Fabrication Process

The fabrication of the SOI-based MEMS actuator is illustrated in Figure 15. The starting material is a silicon-on-insulator (SOI) wafer with the handle layer of 350μm in thickness, a buried oxide (BOX) layer with a thickness of 2μm, and a device layer with a thickness of 10μm. The first step of the process is to pattern a lift-off photoresist layer which defines the comb-drive structure. After the photoresist is patterned, a non-conformal layer of Cr/Aru (20~30nm) is deposited. The metallic layer of chromium-gold will serve the duo purposes of being a hard mask to avoid unwanted removal of silicon during the plasma etching of the device layer, as well as an electrical bottom contact. A lift-off process is used to remove the metal from undesired places in the device (such as the gaps). A deep reactive ion etch (DRIE) is then performed to etch through the 10μm thick device layer using a plasma etch Bosch etch process. At this point, a TMD can now be transferred on to the MEMS actuator. The TMD is mechanically exfoliated from an MoS_2 crystal source and transferred onto the MEMS. Gold is deposited and patterned using an e-beam deposition and lithography process to mechanically clamp the TMD as well as serve as electrical

top contact. At last the structure is released using HF vapor to etch silicon dioxide in areas where the structure needs to be free to move such as the rotor.

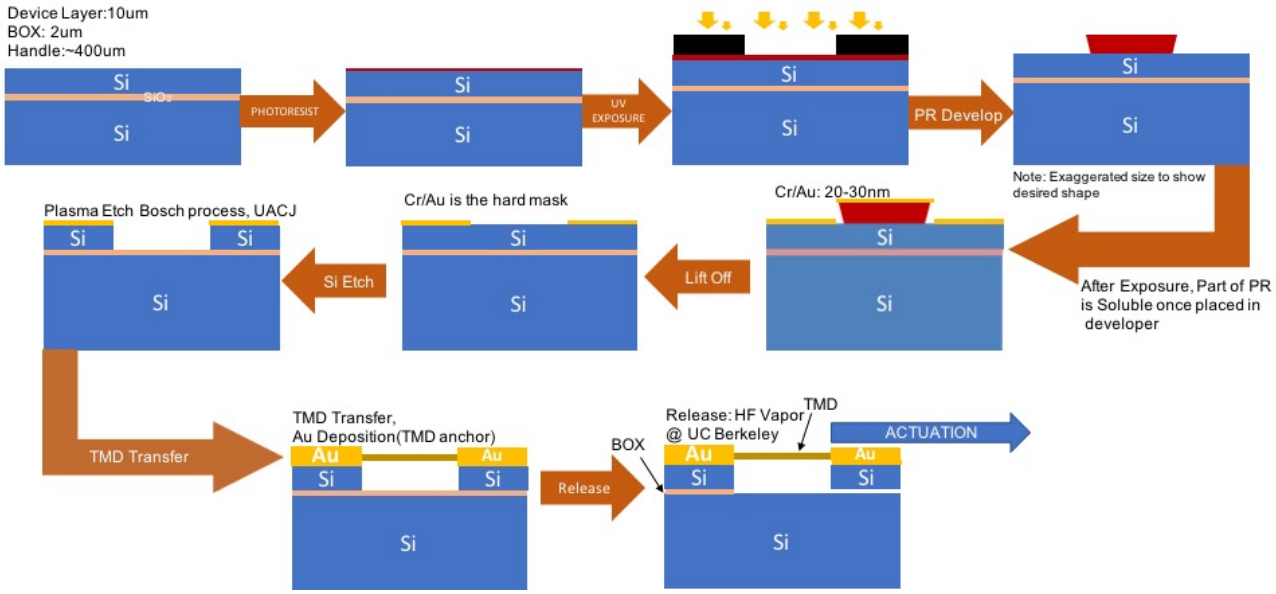

Figure 15: UTEP/UACJ SOI fab process

5.3 SOI Design Parameters

The force balance model given in Equation 8 contains several parameters that must be defined to complete the design. Some of the parameters are fixed and others are tunable. The fixed parameters are due to constraints arising from processing limitations and material selections. One processing limitation is the etch depth-to-width aspect ratio of the SOI device layer. Due to limitations of the Bosch DRIE process, the maximum aspect ratio that can be achievable is 10:1. Since the thickness of the device layer is 10μm, the minimum feature size is 1μm. This means that the minimum feature size of the gaps and other lateral dimensions is 1μm. Therefore, the width of the gap (g) and length of the unstrained TMD (d) are fixed at 1μm as listed in Table 1. Moreover, the thickness of the MEMS actuator is set by the thickness of the SOI device layer which is 10μm. The width of the TMD was selected to be 3μm because this is experimentally a typical width of a TMD flake. Since MoS_2-2L was the TMD material selected for the design, the stiffness of the

TMD is fixed at 182 N/m. Finally, the TMD strain required to achieve 6 orders of increase in conductivity is 6% for MoS_2-2L.

Table 1: Fixed parameters of force balance model of SOI device

Parameter	UTEP-UACJ	Units
ε_0	$8.85\ x\ 10^{-12}$	Fm^{-1}
t	10	μm
g	1	μm
d	1	μm
ε	6	%
w_{TMD}	3	μm
k_{TMD}	182	Nm^{-1}

5.4 SOI DESIGN ALGORITHM

The tunable parameters, which primarily focus on finger and spring characteristics, are important because they affect the actuation characteristics of the device. A design algorithm was developed which takes the fixed parameters and then tailors the tunable parameters to lower the voltage required for the critical strain. The design algorithm is shown in Figure 16. The first step is the consideration of the stiffness of the MEMS. A stiffer structure is more rigid and resistant to deflection and will thus require larger activation voltages. A MEMS with very low stiffness will allow for lower operational voltage, however it will also be more susceptible to component deflections from residual stress. The stiffness of the device is based on certain parameters such as the geometry and materials used (as seen in Equation 5). These include; the Young's modulus of the material (E), thickness (t), width (w), the and length (L) of the springs. E and t are fixed by the material selection and fabrication constraints, however *w* and *L* are tunable parameters.

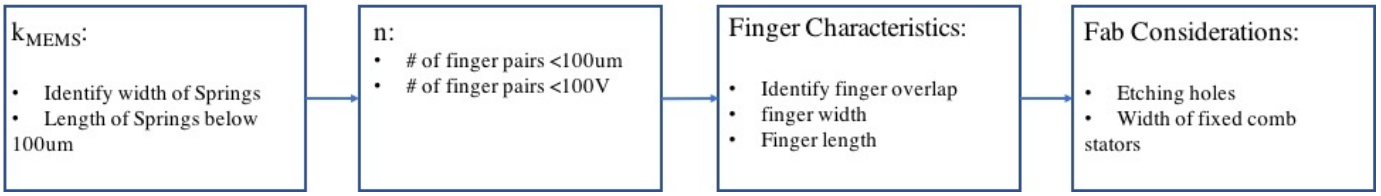

Figure 16: SOI design algorithm

Although the width of the spring is a tunable parameter, a constraint exists that derives from the etch release process that places an upper bound on the width. Components with width above 3μm require etching holes in the structure to facilitate the release of the structure in order to successfully remove the oxide beneath the parts which should be floating. Thus, the width of the spring beams is selected to be 3μm to ensure a good release of the spring without the need for etch holes.

An upper bound was also placed on the length of the springs in order to achieve a compact design and minimize any deflection in the structure due to residual stress from the fabrication process. Since the lateral extent of the actuator was 200μm, this placed a limit to the spring length of 100μm. This value of spring length can be modified later based on the number of finger pairs that can fit into this length in the interest of achieving a compact device.

Based on the constraints derived from the fabrication process (1μm minimum feature size) and the upper bound of the actuator size (100μm), it was determined that 15 finger pairs could be used per comb. In other words, the combs were standardized to consist of 15 finger pairs. This allowed the combs to be approximately 100μm in length. However, what remained to be determined was the number of finger pairs, *n*, (and therefore combs) required to achieve a sub-100 Volt operation. In order to determine *n*, the gate voltage in Equation 8 was plotted as a function of *n* at 6% strain as shown in Figure 17. Figure 17 shows that at least 40 finger pairs are needed to achieve a sub-100 Volt operation. However since there are 15 finger pairs per comb, the minimum

number of combs is 4 since the actuator architecture requires an even number of combs to maintain actuator symmetry. This translates to 60 finger pairs (4 combs X 15 pairs/combs) at a voltage operation of ~80 V. It was decided to also fabricate actuators with twice these number of combs (8) to study the effect of number of combs on actuation.

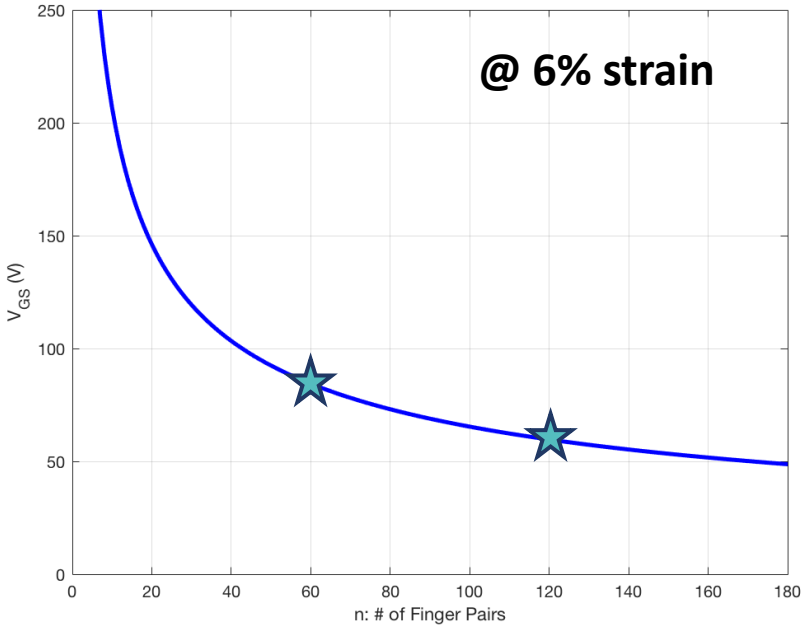

Figure 17: SOI voltage vs. # finger pairs

Finger-overlap is another characteristic that needs to be considered in order to maintain device stability while enhancing the electrostatic force between the charged interdigitated comb electrodes. Based on the capacitive sensing mechanism of the electrostatic comb drive actuator, finger widths and gaps are chosen based on the smallest features which can be realistically fabricated. But as the MEMS actuator is scaled down to achieve energy efficiency, features below a micron enhance other forces that affect the behavior of the device. [30] For example, the effect of the rapidly increasing electrostatic force while weakening strength of the fingers at smaller feature sizes can cause failure of the device due to collapse of the fingers. [30] Reducing the

overlap of neighboring fingers and excessive finger length aide in minimizing instability due to the augmenting axial forces and therefore the risk of collapse amongst the fingers at such small features.

The effect of finger overlap on structure deformation and voltage operation was studied. Figure 18 compares the stresses in combs with 25% and 75% overlap at an applied voltage of 90 Volts. The comb with the 75% overlap has a higher degree of stress compared to the comb with 25% overlap. Although a smaller overlap will reduce stresses, it will also reduce the electrostatic force which leads to larger voltage operation. Considering that augmentation of voltage increases the electrostatic force in the axis of movement (y-axis, in this case) it can also be noted that the force also increases in other axes, such as the x-axis. The increase of force in the x-axis leads to issues with side-instability. The instability becomes significant with longer, slender fingers, and with greater overlap. Therefore, the overlap should be kept as small as possible while maintaining a satisfactory low-voltage operation.

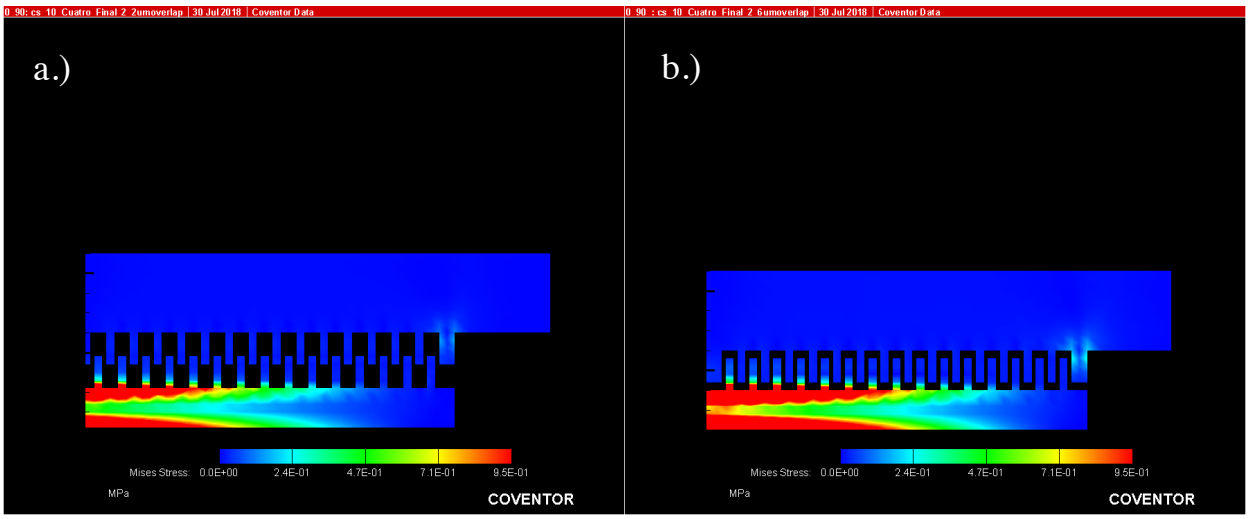

Figure 18: Stress observed at 90 volts a.) 25% finger length overlap b.) 75% finger overlap

The effect of finger overlap on voltage is shown in Figure 19. Upon testing various overlapping lengths, the increase in overlap poses similar results at 25% and 50% overlap. In

contrast, a reduction of ~15 volts are observed at 75% overlap. Taking into consideration the effect of finger overlap on device stresses and voltage operation, the finger overlap for MEMS actuator was selected to be 50%.

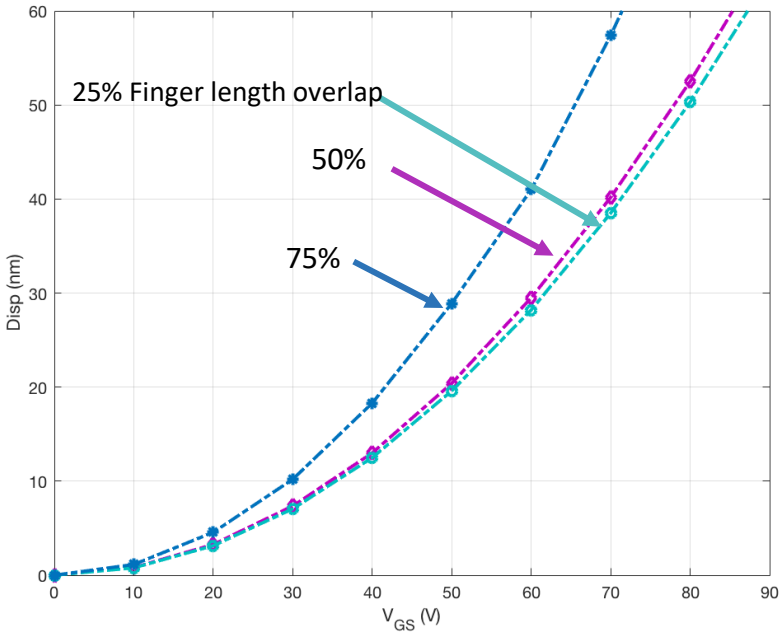

Figure 19: Displacement vs Voltage with varying finger overlap

Finger instability is also observed in the outer fingers of the comb observed in Figure 18. This occurs due to the lack of cancellation of forces in the outer fingers which is present in the middle fingers. The lack of this cancelation of forces can result in the deformation of the outer fingers if they are not made strong enough. [32] To suppress the deformation, the width of the outer fingers was increased compared to those in the middle.

The remaining device design considerations are based on fabrication. As aforementioned, parts of the device with widths above 3µm will require etching holes to promote the feasibility of release. On the other hand, fixed parts of the structure, such as the contact pads, the stators of each

comb, and the truss, will be made sufficiently large to prevent their release upon the removal of oxide.

A list of the resulting design parameters for the SOI design are given in Table 2.

Table 2: SOI design parameters

Parameters	**SOI**	**Units**
E	Si: 130	GPa
W	3	µm
t	10	µm
L	94	µm
$k_{MEMS\ (Analytical)}$	84.52	Nm^{-1}
V	< 100	volts
k_{TMD}	182	Nm^{-1}
# of combs	4, 8	N/A
Finger pairs: n	15 Per Comb	N/A
Finger length	8	µm
Finger width	2	µm
Finger overlap	4	µm
Outer finger width	4	µm
Pad dimensions	100x100	μm^2

5.5 SOI ANALYTICAL MODEL

The displacement as a function of voltage was analytically calculated using the force balance model based on the given parameters in Table 2. Figure 20 plots the displacement as a function of voltage using the analytical model. Figure 20 shows that 6% strain is achieved at ~60 and 85-volt operation with 120 and 60 finger pairs, respectively. This presents an estimate of the voltage of operation required to achieve the necessary strain. Modifications to the final design will ultimately slightly alter these results. However, stiffness of device has minimal effect in the overall voltage applied, due to the domination of the stiffness of the TMD which proves the most difficult to overcome.

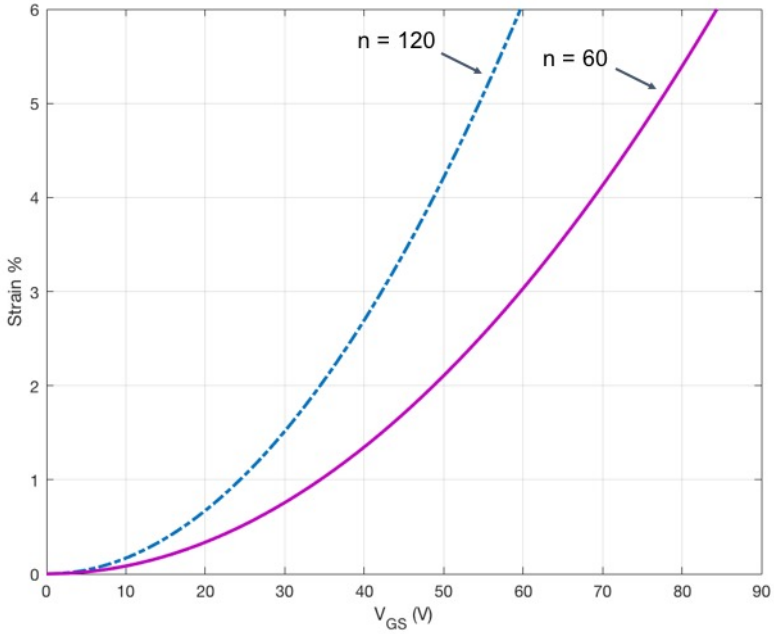

Figure 20: Analytical displacement vs. voltage of the SOI design observed for the 120 and 60 finger pairs. (displacement in terms of percent strain (6% of the TMD gap))

5.6 SOI Simulated Analysis

5.6.1 Introduction

The comb-drive actuator is simulated using the Coventorware software in order to study the device's response. The Coventorware tool emulates the actual device process of design and fabrication of devices. This includes; the materials used for the actuator, fab process, mask layout, and final model testing. The following sections will follow the process flow of the software used to simulate the device.

It is important to note that the process flow of the simulation is an abbreviated version of the real fabrication process shown in Figure 15. The main reason for the deviation between the simulated and real processes is that the TMD is modeled as a spring in simulation and not as a thin material layer. Therefore, all the steps needed to transfer and anchor the TMD in the real

fabrication process are not included in the simulation process. Instead, a linear spring force using the stiffness of a TMD is used to simulate the presence of the TMD. Similarly, other layers used primarily for electrical contacting and anchoring the TMD are not included in the simulation process.

5.6.2 Material Database

The materials employed for the SOI process are single crystal silicon for the structure, and silicon dioxide for the BOX. The properties of the materials such as strength, density, thermal, etc. are essential for analytical and simulation accuracy, therefore if a material is not included in one of the material libraries, it must be imported to the material database based on the values found in literature.

The Cr/Au metal layers are not included in the simulation because they do not contribute significantly to the electro-mechanical actuation of the device. Instead, the metal layers are needed in the real device due to their role in the electrical contacting and mechanical anchoring of the TMD and not the electro-mechanical aspects of the silicon device layer.

5.6.3 Process Editor

The sequential order of the processing steps needed to simulate the device actuation are added to the process editor. The simulated processing flow consists of three essential steps; definition of the starting SOI wafer, lithography and etching of the silicon device layer, and isotropic etch of the BOX to release the device. The first step is to add the SOI layers to the process editor which consist of the device (10 μm), BOX (2 μm), and handle (350 μm) layers. This is followed by a lithographic step that will define where the device layer will be etched using a mask.

Next the device silicon layer is etched using a DRIE process. Finally, the BOX layer is etched using an isotropic process to release the movable parts of the actuator.

Several process steps present in the experimental process (Figure 15) and other effects are not included in the simulated process. For example, deposition of the Cr/Au and Au layers to form the bottom and top contact for electrical enhancement and mechanical purposes in regard to the TMD are not included in the process editor. The electrical properties of the device (i.e. current flow), are not simulated, and the mechanical anchoring of the TMD from the metal contacts is not needed in the fabrication process file. Similarly, the experimental scalloping of the walls upon the DRIE are not considered in the process editor.

5.6.4 Layout Editor

Upon the selection and creation of the materials and process of fabrication respectively, the masks pertaining to the SOI process must define the geometry of the device. Therefore, the 2D analytical blueprint must be created in the design layout and include the different masks designs employed by the process. The SOI design consists on a single mask process which avoids deposition of sacrificial layers and multiple masks to define the anchored components.

Figure 21 shows the four and eight comb model of the actuator, with the unique design characteristics for the SOI design, complying with the characteristics given in Table 2. In order to aid in the release of the structure, the fixed components such as the stator of each comb is doubled in width compared to those which are free, such as the rotor of each comb, and the truss of the structure. Anchored parts of the device are defined based in an experimental process, tuned according to the etch rate of silicon in order to determine the time and conditions needed to release the device. However, the needed boundary conditions will be added later to the 3D model to specify anchored and free parts of the device.

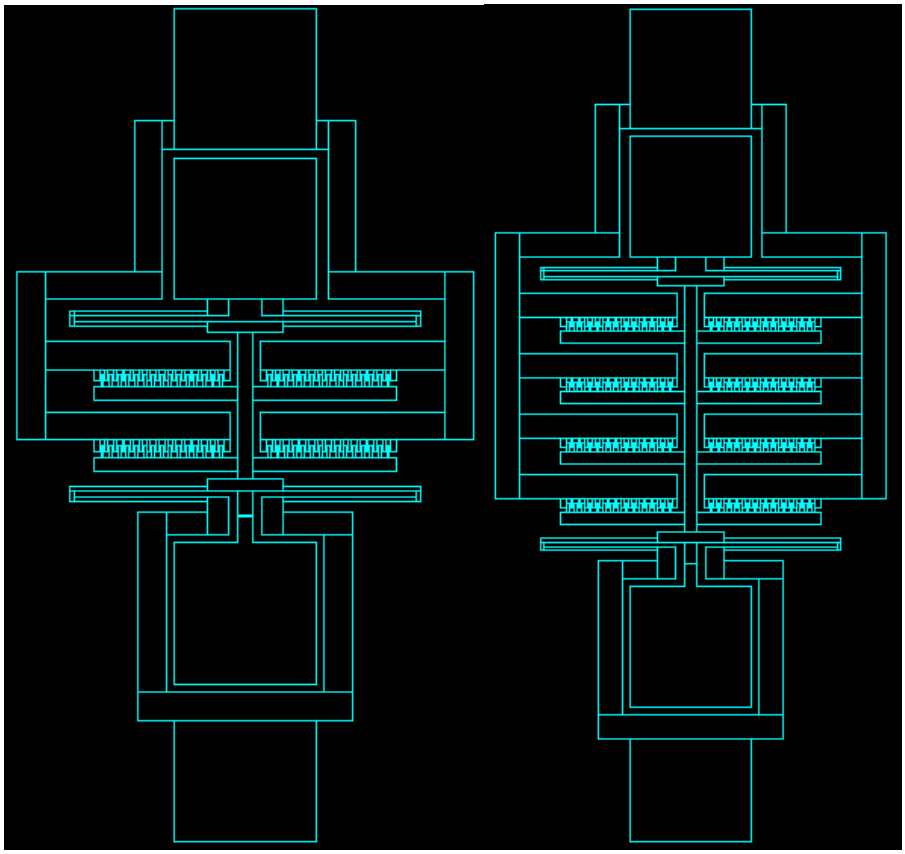

Figure 21: 4 & 8 SOI comb designs

5.6.5 3D Model

Figure 22 illustrates the final 3D model, with the different areas of the actuator defined. The simulation accuracy is based on the quality of the mesh selected for the 3D model. Various meshes with different parameters are selected in order to choose the best one for the SOI considering the trade-off between the computational cost and accuracy.

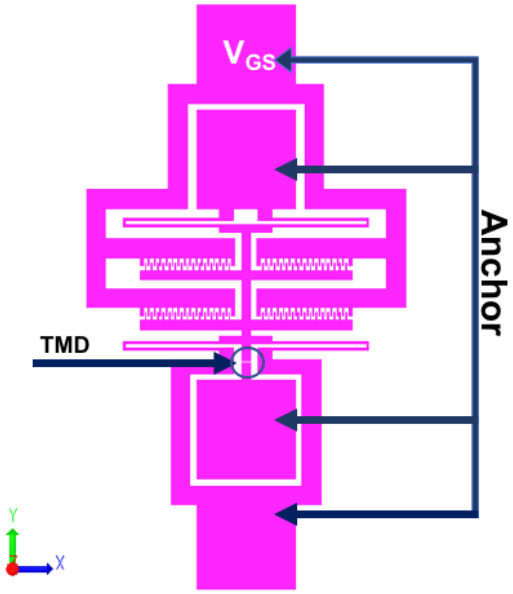

Figure 22: 3D SOI model

5.6.6 MemMech Analysis

The accuracy of a simulation depends on the quality of the mesh employed. Finer meshes give more accurate results but are more computationally expensive. Therefore, a trade-off must be found between the accuracy and computational cost. In this work, the stiffness of the actuator springs is a crucial parameter in the operation of the device that was used to gauge the accuracy of simulation results. This was done by comparing the stiffness calculated from an analytical equation (Equation 5) to the stiffness predicted from simulation using different mesh sizes. The stiffness of the MEMS is a crucial characteristic of the actuator since it determines the MEMS' resistance to deformation upon the application of a load.

MemMech which is the mechanical solver for the software was used to determine the stiffness of the MEMS from the simulation. MemMech enables the mechanical analysis of MEMS structures, such as prediction of displacement from applied forces. A 10μN force was applied in

the direction of actuation (y direction) and the displacement was measured. Hooke's Law was then used to determine the stiffness by dividing the force by the displacement.

Table 3 contains a comparison between analytical and simulation computed stiffness using 3 different mesh element sizes created for the 4-comb design. Mesh 2 presents a good trade-off between accuracy and computation cost and was chosen for the device simulations. The accuracy of the mesh can be further verified based on the comparison between simulated and calculated work. Mesh 2 can be viewed in Figure 23.

The stiffness of the device is given based on the results of the 4-comb design, however due to the same geometry and dimensions of the 8-comb, the stiffness should remain the same. However, the computation time is expected to increase for the 8-comb, as well as a slighter % error. This is due to its greater degree of complexity and the need for an optimized mesh for each design.

Table 3: SOI mesh characteristics

Mesh	**Element Size (x,y,z)**	**Aspect ratio: range**	**Aspect ratio: average**	**Sim. Time (Memory: 3000MB)**	**Stiffness *(N/m)***	**% Difference Sim vs. Analytical**
1	3,3,3	[1,2]	1.17	00:00:44	93.25	10.32%
2	**2,2,2**	**[1,1.5]**	**1.03**	**00:04:42**	**92.11**	**8.98%**
3	1.2,1.2,1.2	[1,1.6]	1.06	00:59:35	91.19	7.89%

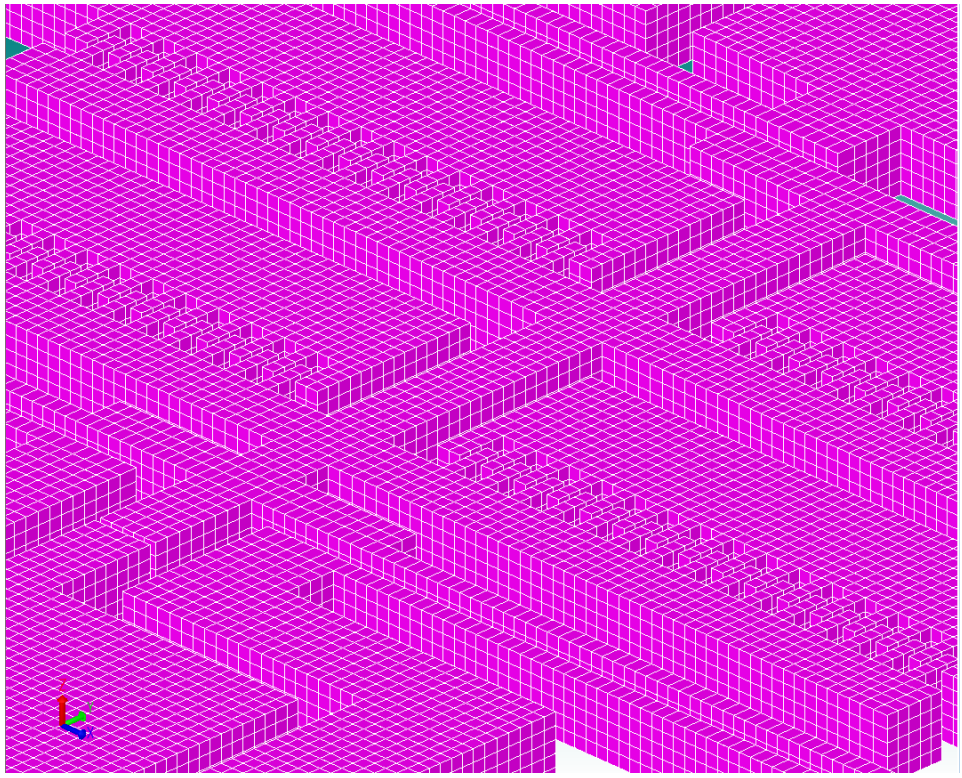

Figure 23: SOI mesh

5.6.7 CoSolveEM

The CoSolve electromechanical solver is used to obtain the displacement of the device based on the applied voltage. This simulation can be computationally extensive and take a considerable amount of time, as a result the accuracy of the applied boundary conditions are crucial in the capture of accurate results. The boundary conditions include the defining of fixed components, as well as the application of the TMD. As the voltage applied induces the displacement of the movable electrode, the TMD behaves as a spring which resists the electrostatic force. The spring model used for the TMD is applied as a boundary condition, where the load will be given based on the force of the TMD. The boundary condition must be given in terms of displacement and not strain, therefore the force of the TMD varies slightly compared to the one

given in Equation 6. Given in terms of displacement the TMD force changes to Equation 9, where x is the displacement, and d_{TMD} is the gap where the TMD will be placed.

$$F_{TMD} = \frac{k_{TMD}\, w_{TMD}\, x}{d_{TMD}}$$

Equation 9: TMD Mechanical spring force in terms of displacement

Given the applied boundary conditions, the effect of the voltage on the 4 and 8-comb can be visually observed in Figure 24, in steps of 20 volts, and given analytically in Figure 25.

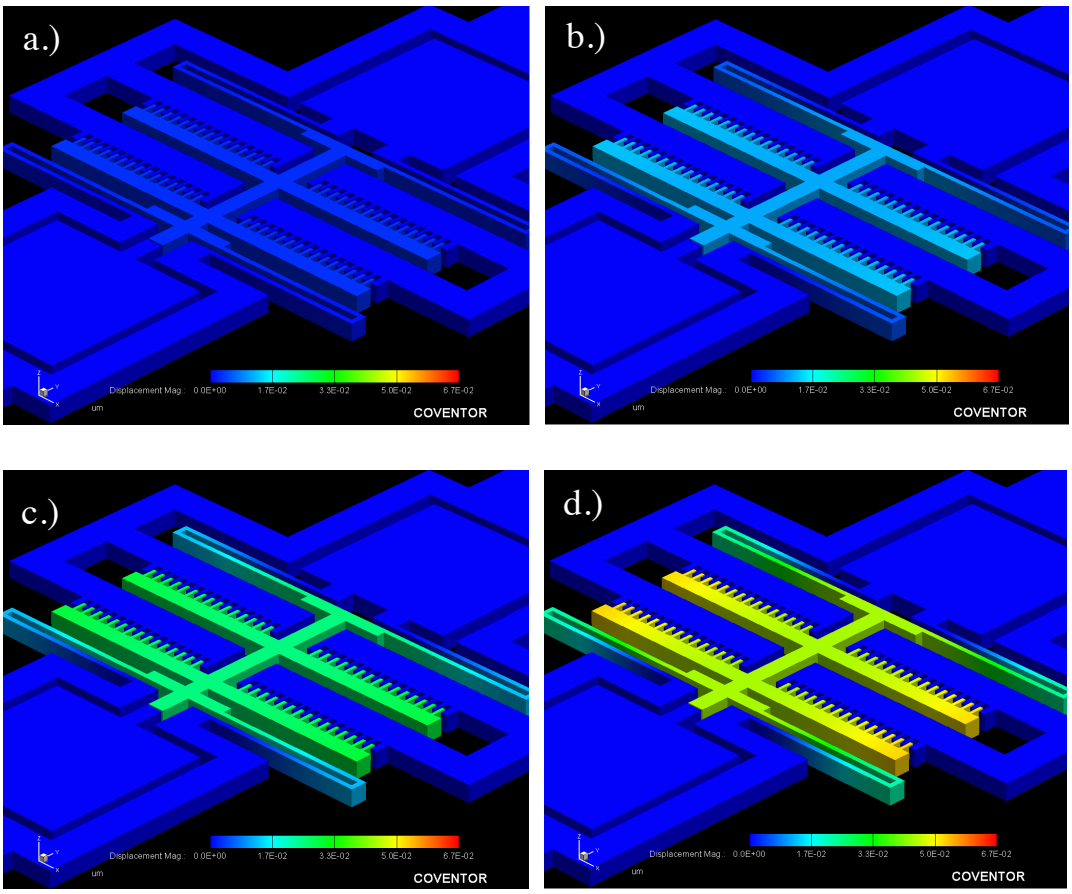

Figure 24: SOI 4 Comb Voltage Vs Displacement a.) 20 volts. b.) 40 volts c.) 60 volts d.) 80volts

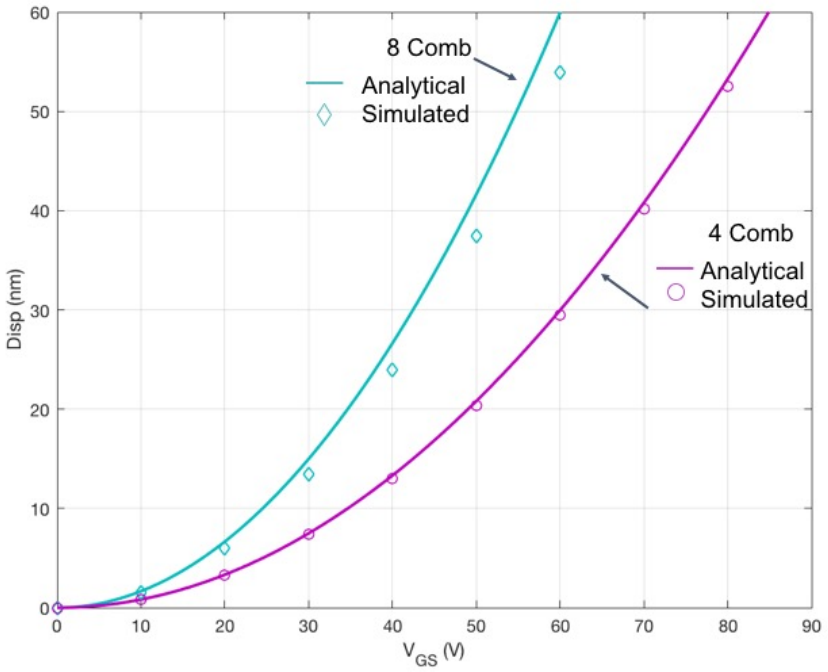

Figure 25: SOI 4 & 8-comb simulated vs. analytical voltage vs displacement

Chapter 6: SiGe Design

6.1 Introduction

The SiGe device is fabricated at UC Berkeley and similarly to the SOI, the understanding of the process is significant to attain final device characteristics. Adjustments to the design are critical to optimize the silicon-germanium device based on the characteristics of the fabrication process. Device optimization will allow to reach the desired critical strain below the 100 volts range.

6.2 SiGe Fabrication Process

The UC Berkeley SiGe MEMS actuator fabrication process is illustrated in Figure 26. The starting material is a silicon wafer. A layer of Al_2O_3 (~80nm) is deposited via Atomic Layer Deposition (ALD) to isolate the substrate. The first sacrificial layer is deposited, a low temperature oxide (LTO1 ~ 600nm) is deposited via Low-Pressure Chemical Vapor Deposition (LPCVD). LTO1 is patterned to define the anchored parts of the device, such as the pads and stator of the comb drive. The conformal deposition of the device layer, silicon germanium ($Si_{.4}Ge_{.6}$ ~1.65um) is done via LPCVD. A second sacrificial layer (LTO2 ~ 100nm) is deposited, and the silicon germanium is patterned to define the structure of the device. A non-conformal layer of Cr/Au (10~40nm) is deposited (to serve as bottom contact) followed by a lift-off process to remove the metal from undesired areas such as the gaps. The TMD is then transferred onto the device after being mechanically exfoliated from a crystal source. The TMD is anchored by the deposition of a layer of gold (~20nm) which also serves as electrical top contact. Lastly the structure is released using HF vapor to etch the silicon dioxide from areas which are free to move.

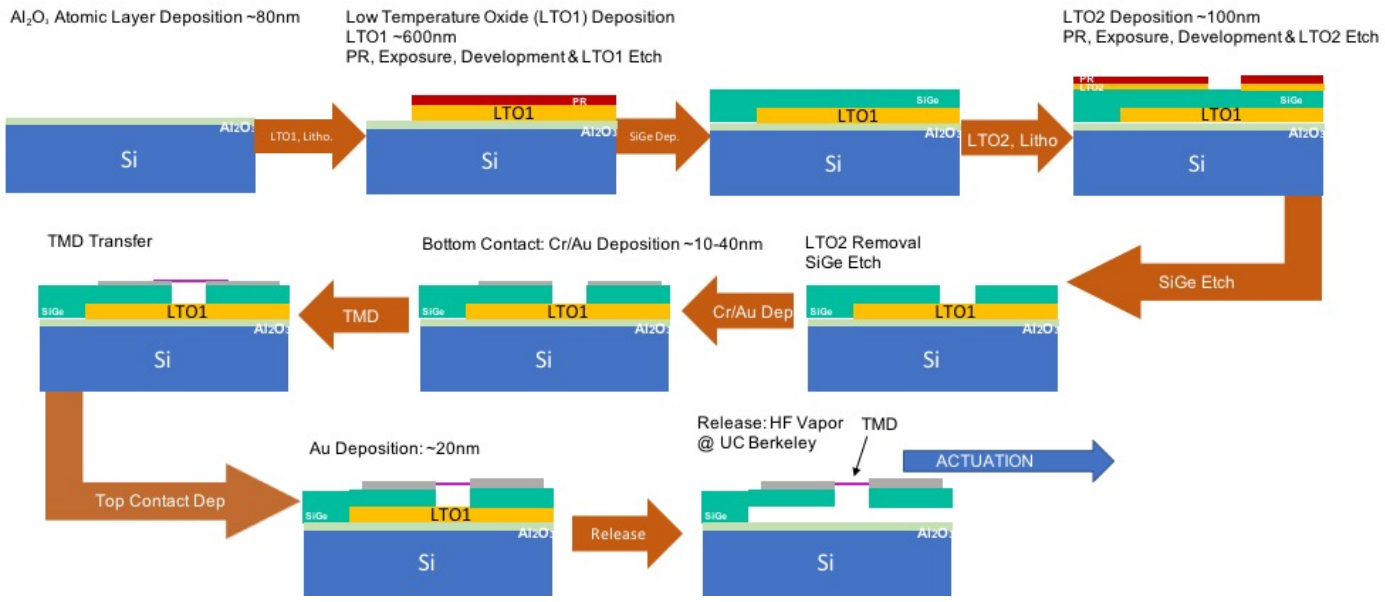

Figure 26: SiGe fabrication process

6.3 SiGe Design Parameters

Given the force balance model of the design (given in Equation 8), various parameters must be determined to obtain the device's characteristics. The fabrication process defines a number of parameters. Differences between the fixed parameters of the SOI and SiGe exist due to the distinct fabrication capabilities and materials. The established UC Berkeley process sets the thickness (t) of the SiGe device to 1.65µm (about six times less than that of the SOI device). The minimum feature size of the process is .5µm, therefore the gaps of the SiGe, both finger gap (g) and length of the unstrained TMD (d) are half of those corresponding to the SOI as seen in Table 4. Similar to the SOI, the width of the TMD (w_{TMD}) is chosen to be 3µm due to its experimentally common width among TMD flakes. The TMD stiffness remains the same, at 182 N/m. The established parameters of the SiGe device will have a different effect on the actuation compared to the SOI. Based on Equation 8 the reduction in thickness of the SiGe will lessen the electrostatic force,

however the reduction in gap size will allow to neutralize and boost the force to counteract modest contribution resulting from the thin structure in order to achieve the 6% of strain.

Table 4: Fixed parameters of force balance model of SiGe device

Parameter	UC Berkeley	Units
ε_0	$8.85\ x\ 10^{-12}$	Fm^{-1}
t	1.65	μm
g	.5	μm
d	.5	μm
ε	6	%
w_{TMD}	3	μm
k_{TMD}	182	Nm^{-1}

6.4 SiGe Design Algorithm

The design algorithm for the SiGe device is the same as the SOI, given in Figure 16. The tunable parameters of the actuator (i.e. finger and spring characteristics) are the most important aspect of the MEMS due to their effect on the actuation of the device. The design algorithm tailors the characteristics for each device in order to reach the critical strain at low voltages. The stiffness of the MEMS is the first step in design. The stiffness is based on material properties and geometry, presenting both fixed and tunable properties. Fixed parameters include the Young's modulus (E) of the material, as well as the thickness (t), while tunable parameters are the width (w), and length (L) of the springs.

The width (*w*) of the springs is chosen to be 3μm based on the same principle given for the silicon device. Due to the necessity to include etching holes in regions of width above 3μm to ease the release of the structure, the width of the springs is maintained at this value.

Given the thickness of the device and feature sizes which are considerably smaller than that of the silicon device, shorter springs are selected. This is done to avoid the propensity of

deflection in different areas of the device resulting from residual stresses from fabrication. An upper bound is placed in the length of the SiGe spring to be 50μm. The length of the springs is ultimately chosen based on the length of the comb. This is done to achieve a compact device where its components are similar in length and overall consistent in their geometry while operating below 100 volts.

Given the constraints of the spring length (~50μm) and minimum feature size (.5μm), it was determined that 20 finger pairs could be used per comb. In order remain within the limitations set by the spring length and feature size, 20 finger pairs per comb give a length of 55μm. To achieve a sub-100 Volt operation similar to that of the SOI, *n,* or the number of finger pairs must be defined. The gate voltage from Equation 8 was plotted as a function of the number of finger pairs for the SiGe device to identify *n,* in Figure 27. Figure 27 shows that at least 140 finger pairs are needed to achieve sub-100 Volt operation. However, an even number of combs is crucial to maintain symmetry, therefore, 160 finger pairs are selected (8 combs X 20 pairs/combs). Selecting 160 finger pairs will allow a voltage of operation of ~85 Volts.

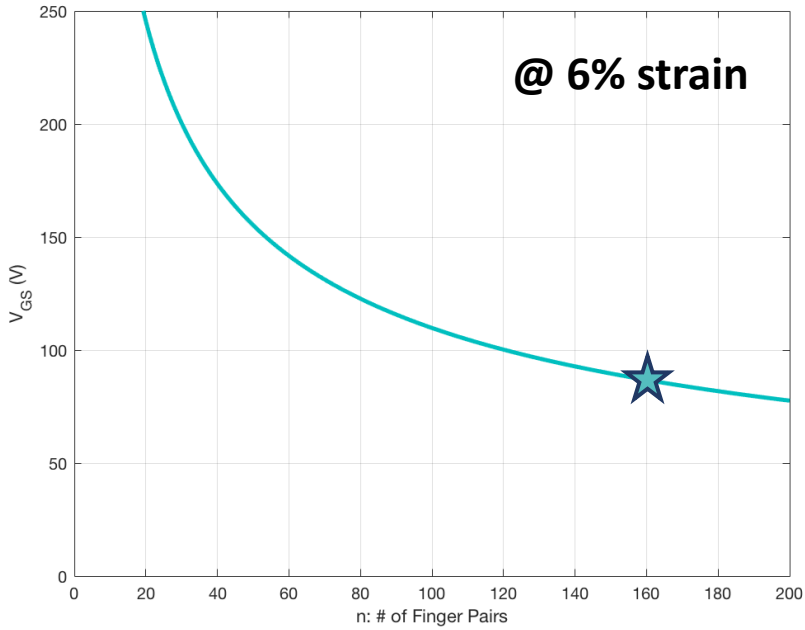

Figure 27: SiGe finger pairs vs. voltage

Finger characteristics are selected based on the fabrication capabilities, and material parameters. Based on the smaller feature size of the SiGe device the finger overlap is reduced to be to be less than 50% of the finger length. Given the small difference in actuation voltage between the 25% and 50% overlap the SiGe overlap is reduced to be closer to the smaller % overlap. A smaller % overlap is selected for the SiGe in comparison to the SOI due to the rising proclivity of finger instability. Minute features, and thin structures have a higher tendency to face issues with instability leading to failure, this is due to the large increment of electrostatic force in comparison to lower stiffness ratio of the device. The reduction of overlap and finger length diminishes possibility of collapse amongst the fingers.

In the pursuit to prevent recurring failures observed within the comb drive actuators, the outer fingers of the comb are made wider than the fingers in the middle. This is due to the lack of cancellation of forces in the outer fingers that can lead to their deformation. Therefore, to reduce

the propensity of deflection in the outer fingers, their width is increased (i.e. to make them stronger).

Some remaining device considerations are established based on the fabrication process. Etching holes are placed in wide parts of the device (those greater than 3um) to enhance the release of the suspended rotor. The mask devised to establish the fixed areas allow the stator and anchored areas of the device to be reduced compared to those of the SOI process, such as the stators of the combs.

The resulting design parameters for the SiGe design are given in Table 5.

Table 5: SiGe design parameters

Parameters	**SiGe**	**Units**
E	152	GPa
w	3	μm
t	1.65	μm
L	55	μm
$k_{MEMS\ (Analytical)}$	81.4	Nm^{-1}
V	< 100	volts
k_{TMD}	182	Nm^{-1}
# of combs	8	N/A
Finger pairs: n	20 per comb	N/A
Finger length	5.5	μm
Finger width	1.5	μm
Finger overlap	1.5	μm
Outer finger width	2.5	μm
Area of pads	100x100	μm^2

6.5 SiGe Analytical Analysis

Utilizing the force balance model and the given parameters for the design in Table 5 the device displacement as function of voltage is analytically calculated. Figure 28 plots the displacement as function of voltage for the silicon germanium model. This plot presents an

expected voltage for the 6% strain of the TMD using the SiGe model. Only one variation of finger pairs is used (160 finger pairs) which shows that the critical strain is reached at ~85 Volts.

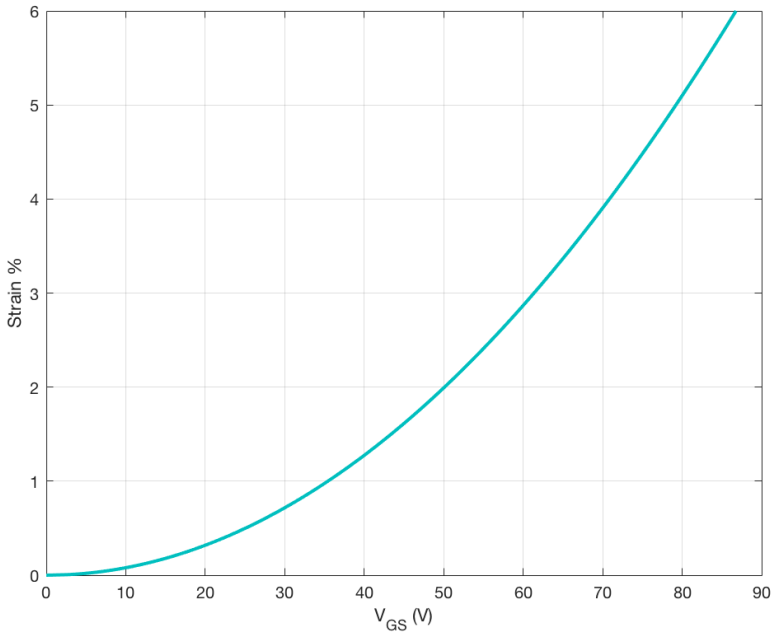

Figure 28: Strain vs voltage of SiGe device (percent strain regarding the TMD gap)

6.6 SiGe Simulated Analysis

6.6.1 Material Database

The materials used for the SiGe process are silicon germanium (SiGe) for the structure, aluminum oxide for the isolation of the substrate (Al_2O_3), and silicon dioxide for the sacrificial layers. The metallic layers used for electrical enhancement and mechanical clamping will not be included in the process and therefore not necessary in the material database.

6.6.2 Process Editor

The poly-SiGe device consists of a three-mask fabrication process which includes the use of sacrificial layers to define anchoring as well as the structure. Similar to the SOI process, the

electrical contact metal layers are not included due to their main contribution in the electrical and mechanical anchoring properties, limiting their impact on the simulated analysis. Due to the elimination of the metal layers in simulation, only the anchor and device masks will be employed for the process. The sequential order of the processing steps begins with a silicon wafer to which Al_2O_3 (~.08 μm) is deposited to isolate the substrate, followed by the first sacrificial low temperature oxide layer (~.6 μm). Upon the deposition of the oxide and first sacrificial layer, a lithography step follows, using the first mask to etch the LTO in order to define anchoring. The deposition and patterning of the device material, silicon germanium (~1.65 μm) (LTO2 is not added, since it is used to prevent the SiGe layer from being etched in unwanted areas upon fabrication, not observed in simulation study). Lastly the structure is released, and due to the "anchor" mask, the software allows for easier definition of fixed areas in the 3D model.

6.6.3 Layout Editor

The 2D layout editor was used to define the two masks used in the SiGe process. Figure 29 shows an overlay of the two masks in accordance with the set parameters given in Table 5. The blue of the mask layout defines the anchored areas whereas the pink layout defines the device structure.

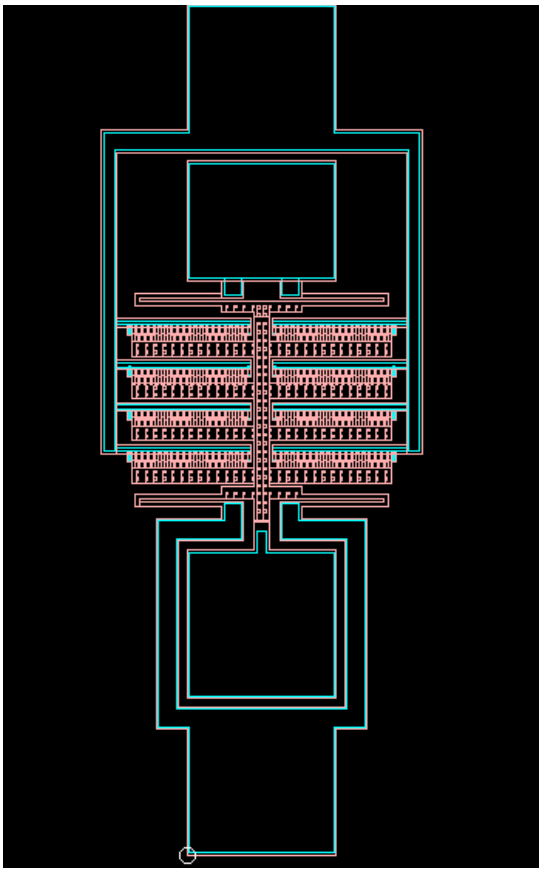

Figure 29: SiGe mask layout

Large anchored areas do not contribute any useful information of the operation characteristics of the device but are needed for probing the real device. However, the large anchored areas incur a computational cost proportional to their size. Since a fine mesh will be needed to capture accurate results due to the thinness of the device, the large anchored areas are computationally very expensive without contributing information regarding the actuation mechanism of the device. Therefore, a reduced mask layout with the large anchored areas eliminated was employed as shown in Figure 30 to reduce the simulation time.

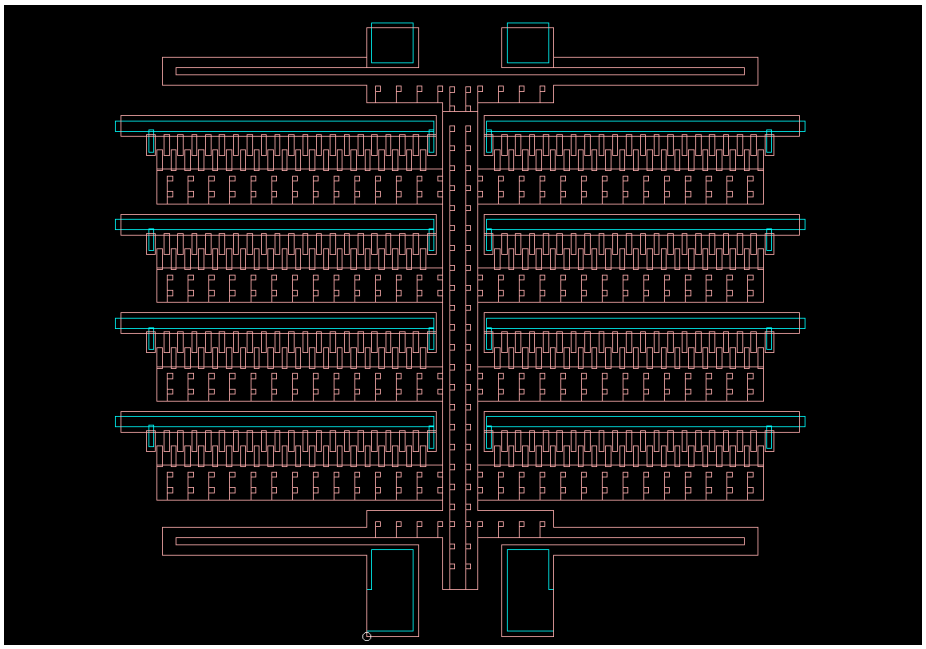

Figure 30: SiGe reduced mask layout

6.6.4 3D Model

Once the 3D model is built, only the layers subject to analysis will be included in the mesh model. Before the creation of the mesh, areas of the device which will be further analyzed or remain fixed must be named. Figure 31 illustrates the different regions of the device which specify which areas are anchored, as well as where the TMD will be placed.

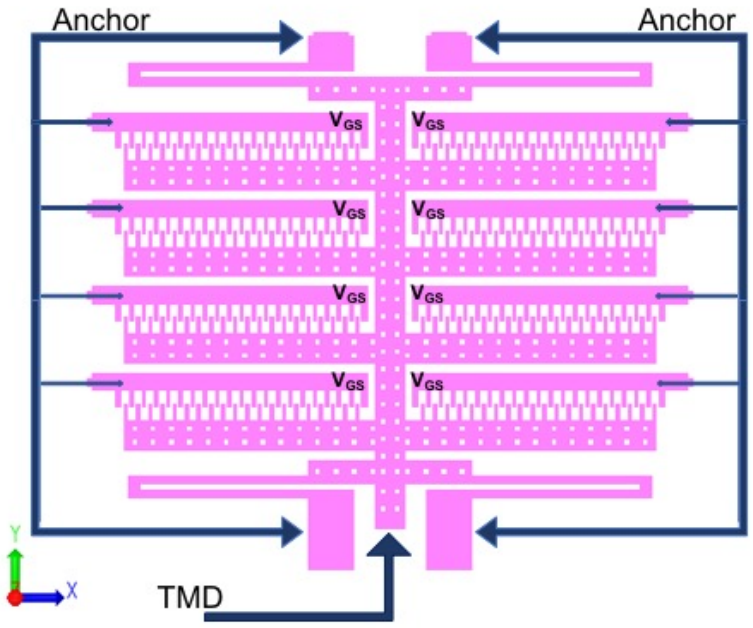

Figure 31: 3D SiGe model, Vg, anchoring, TMD

6.6.5 MemMech Analysis

MemMech will aid in simulating the SiGe's device's stiffness. Stiffness is a critical parameter for MEMS in order to identify the device's voltage requirements, as well as its response to large loads. Hooke's Law is used to identify the simulated value of the device's stiffness. Just as was done for the SOI device, a load of 10μN is applied in the axis of actuation (y-axis). The load was then divided by the displacement in order to obtain the stiffness.

Given in Table 6 are the results and characteristics for 3 meshes. A seen in the table, 3 meshes were tested, with differing element size, and aspect ratios, and ultimately different results in their simulations. In comparison to the SOI device, a thicker device can allow less refinement and obtain greater accuracy than a thinner one. In order to have similar number of mesh elements and therefore calculation nodes, the element size must be greatly reduced in thinner structures. The two initial meshes are Manhattan bricks, while the third mesh is a tetrahedron mesh. The

Manhattan bricks mesh does not allow for higher degrees of refinement in specific areas, and therefore would require very small element sizes. Given the large area of the device, minuscule element sizes would require substantial computational power. The tetrahedron mesh allows refinement in specific areas, therefore reducing the computational needs.

In order to reduce the computational cost required to improve accuracy, the tetrahedron mesh's was given a finger element size of 0.2µm, while the rest of the device was left at 1.5µm (observed in Figure 32). The third mesh was chosen due to the smallest % error given in comparison to the other meshes.

Table 6: SiGe mesh characteristics

Mesh	**Element Size (x,y,z)**	**Aspect ratio: range**	**Aspect ratio: average**	**Sim. Time**	**Stiffness *(N/m)***	**% Difference Sim vs. Analytical**
1	1,1,1	[1.03,11]	1.97	00:00:44 (3000MB)	63	22.6%
2	.55,.55,.55	[1,7]	1.47	00:02:38 (3000MB)	61.6	24.32%
3	**Fingers: .20 Other: 1.5**	**[1,13.9562]**	**1.71**	**00:25:37 (10,000MB)**	**95.02**	**16.73%**

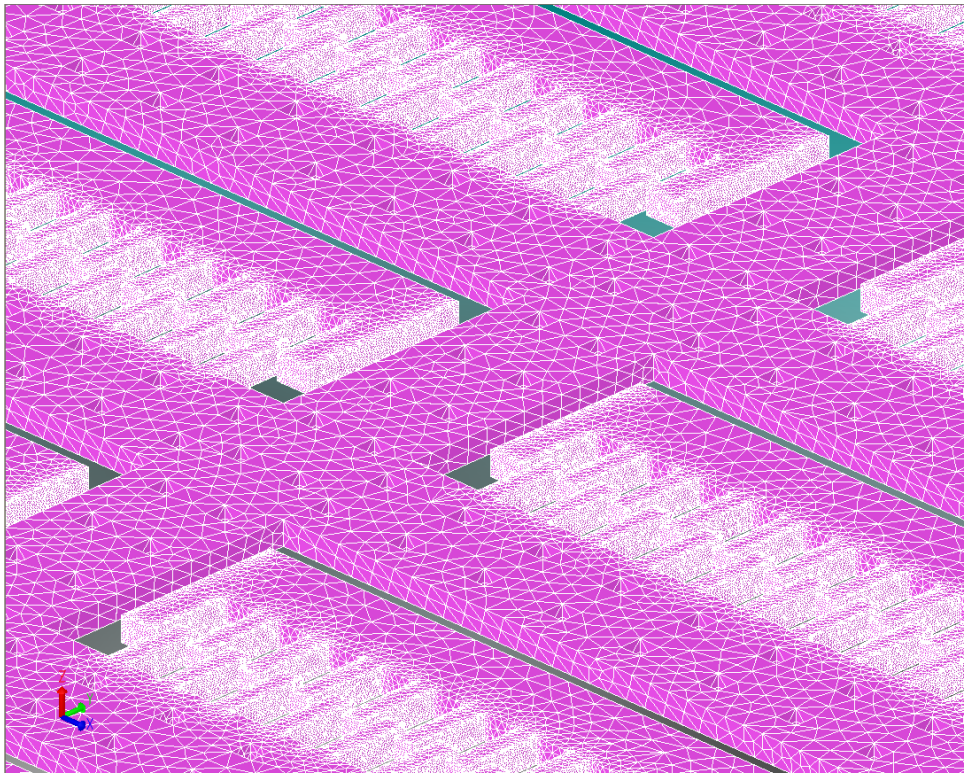

Figure 32: SiGe mesh

6.6.6 CoSolveEM

The CoSolve electromechanical solver is once again used to obtain the displacement of the device based on the applied voltage. The boundary conditions are used to define the fixed parts of the device, the placement of the TMD, and where the voltage is applied. Similar to the SOI the boundary condition of the TMD, it is applied using the force of the TMD based on Equation 9.

The simulation results can be visualized in Figure 33. The image illustrates the effect that 80 volts (we require about ~85 volts to reach 6% strain of TMD), has on the structure. The deflection observed at the edges of the comb-rotors is greater than that observed for the SOI at the same voltage. The thinness of the device augments the propensity for deflection in various areas, such as the edges of the device, this can be attributed to the greater effect that forces, and stresses

has on the comb. Figure 34 illustrates the voltage vs displacement of the structure, both the simulation and calculated results.

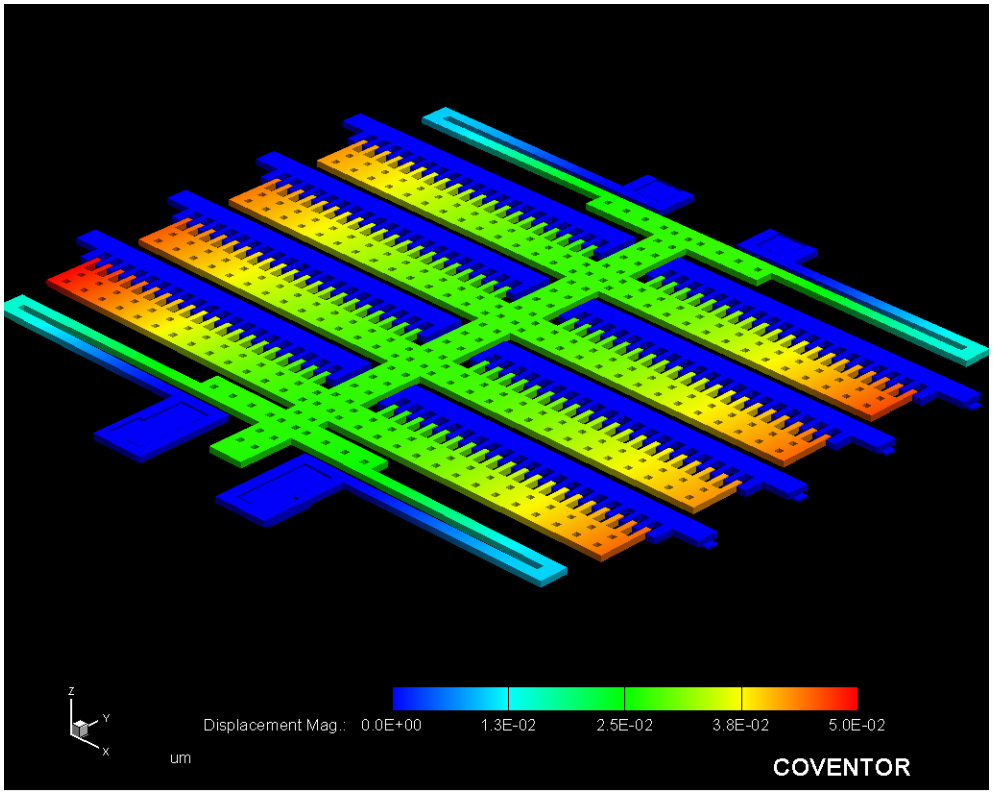

Figure 33: SiGe comb displacement @ 80 volts

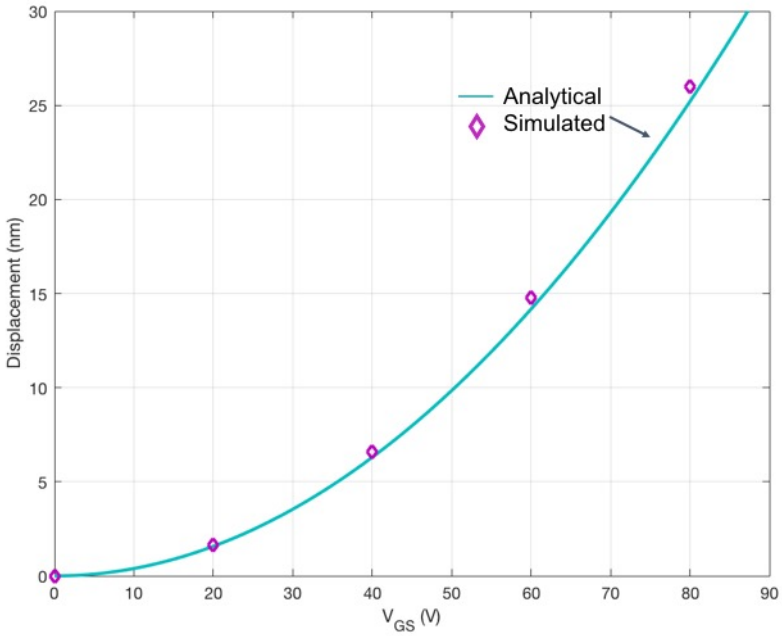

Figure 34: Voltage vs Displacement of SiGe device

6.7 SOI & SiGe Comparison

The SiGe device also has a greater displacement in the z-direction than that encountered for the SOI design. At the maximum voltage of 90 volts, the SOI device actuated about 0.037nm, while the SiGe device actuated about 9nm at 80 volts. This is due to the thinness of the device, but very importantly, the thickness of the oxide between the substrate and device layer. Once the oxide is removed, forming a smaller gap between the device and substrate augments the capacitance between the components, in this case in the z-direction. Therefore, a greater displacement is achieved in the vertical direction when applying the voltage to the comb stators of the SiGe than the SOI. Vertical displacement could also be considered a form of actuation, due to the large area of the device, and small gap between the device and substrate. Voltage applied to the substrate can aid in the use of lower voltage. Vertical actuation can be accomplished by the modeling of the comb-drive as a parallel plate capacitor between the substrate and the device layer (as observed in

Figure 35). The application of the voltage to the substrate will pull down the device, this can enable actuation at lower voltages.

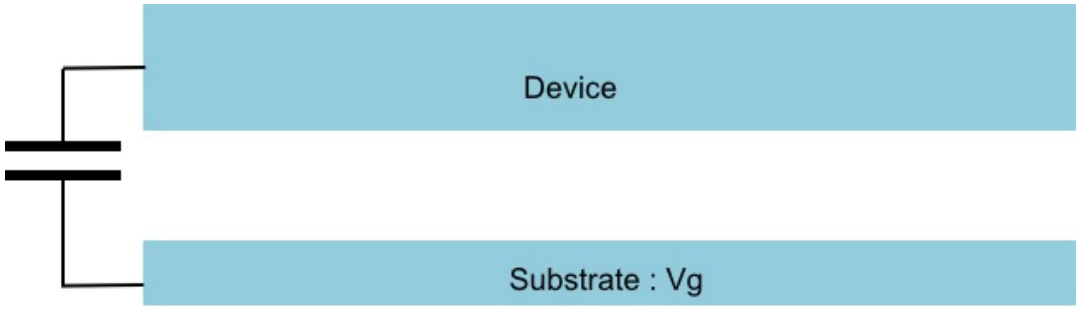

Figure 35: SiGe capacitor between substrate & device

Upon the simulation of the vertical actuation with the properties established in Table 7, the device pulls in to the substrate (600nm gap) at 7-8 volts. This can be visualized in Figure 36, where the greater amount of displacement is observed in the middle to end of device, due to the resistance presented by the application of the TMD. However, this mode of actuation can be utilized for lower actuation voltages in comparison to the lateral actuation used currently.

Table 7: Vertical actuation characteristics

Parameters	**SiGe**	**Units**
t	2.4	μm
k_{TMD} (1L-MoS2)	124.24	Nm^{-1}
g	.6	μm

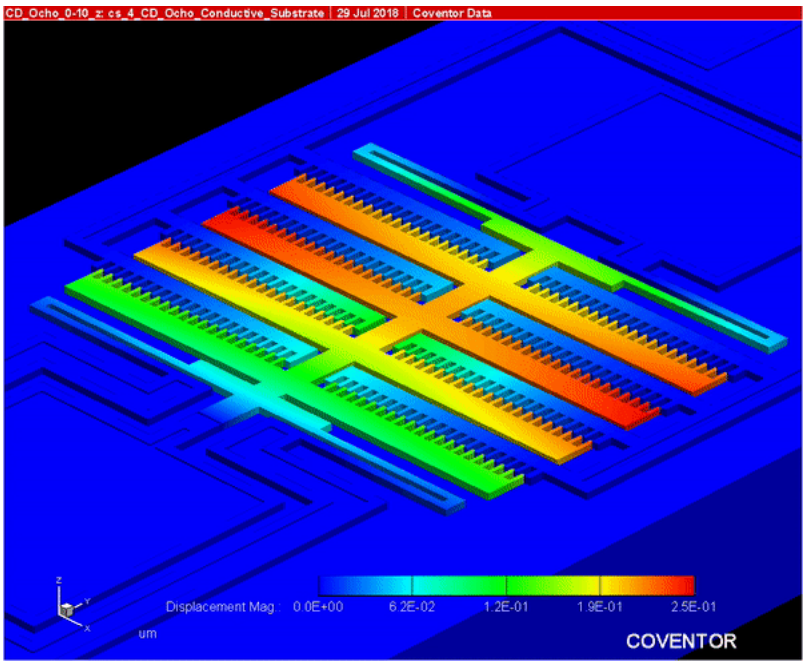

Figure 36: Vertical actuation SiGe device (0-6 volts)

Stress upon the structure is also considered and compared between the SOI and SiGe devices, due to the effect that stress has on devices that leads to failure. Due to the spring-like nature of the device the greater degrees of stress are expected to be in the movable regions, such as the springs due to the deformation they experience, as well as in the rotors. Stress can illustrate the areas of the device most susceptible to deformation, whether desired (such as in the springs) or undesired (in areas such as the fingers). In Figure 37, we can observe the overall stress in all of the device, while in Figure 38, we can see a closer look at the stress in the fingers. Overall the SiGe device experiences a greater degree of stress in comparison to the SOI. The thickness of the device aides in the stability of the overall device. While also considering that the effect of high voltages on slimmer, thinner fingers leads to the propensity of greater stress and likelihood of finger stability.

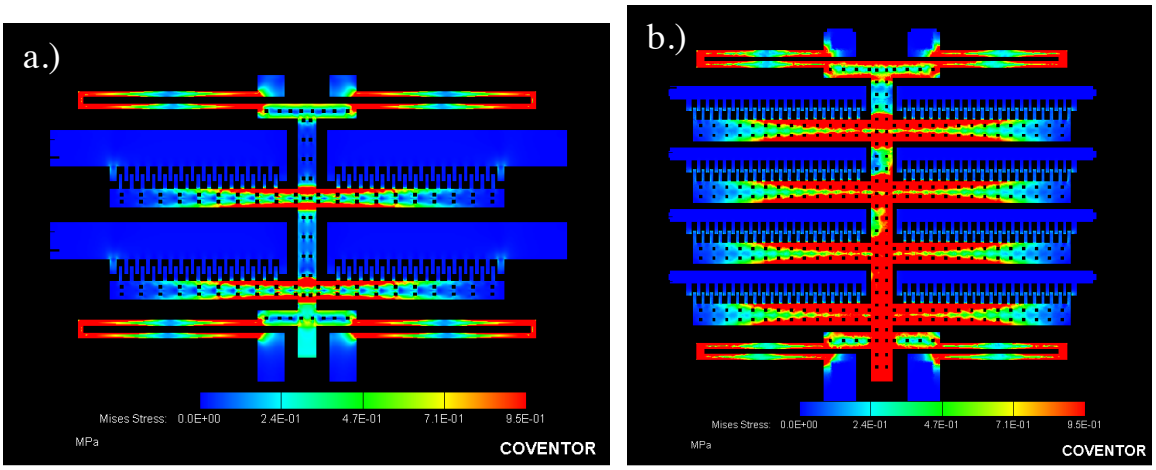

Figure 37: Stress comparison: a.) SOI @ 80 volts b.) SiGe @ 80 volts

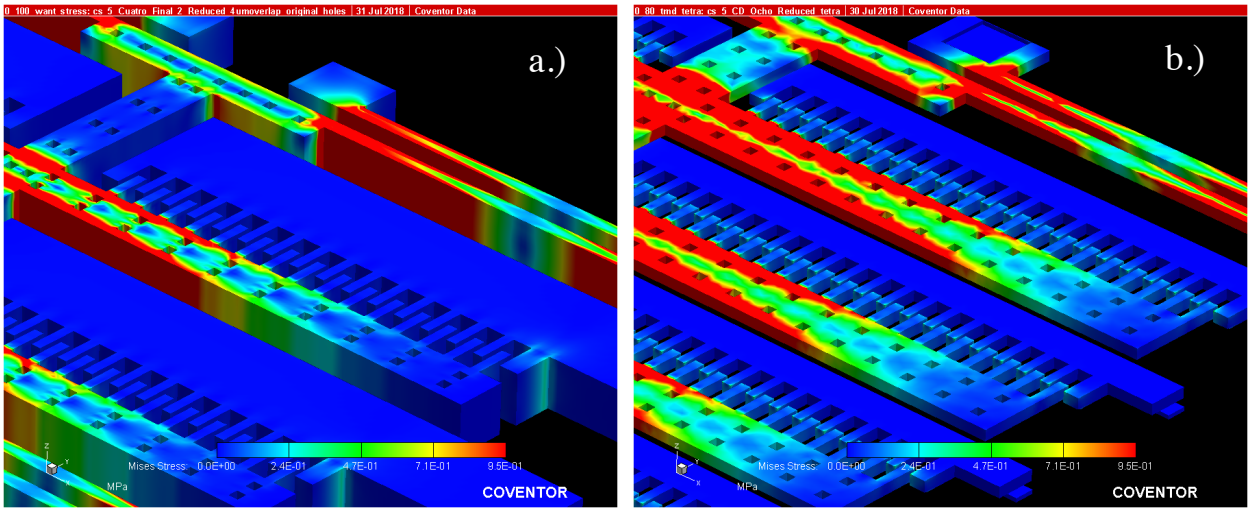

Figure 38: Stress comparison in fingers: a.) SOI @ 80 volts b.) SiGe @ 80 volts

Chapter 7: Conclusion

The work of this thesis consisted in the design and simulation of MEMS actuators to strain 2D materials up to 6%, while optimizing the desigs based on available fabrication capabilities.

In the SOI design, overall material thickness aides the stability and resistance of out-of-plane deflections, and overall propensity of stress. This is compared to the thinner SiGe device which experiences greater out of plane displacement, and overall greater degrees of stress. Thickness of the device also enhances the electrostatic force to lower the actuation voltage in the SOI design, while the SiGe counteracts this with the smaller gaps in the combs. The finger overlap should be maintained within a 25-50% overlap to reduce the propensity in side instability of fingers observed at higher percent overlap, particularly in the SiGe device. The SiGe device should have smaller overlap in the fingers due to the greater susceptibility of slimmer, thinner fingers to stress from large loads. Vertical actuation is an alternative mode of actuation for the SiGe, which can enable lower voltages and greater displacements.

The meshing of the devices which can enhance or diminish accuracy of the simulation results should be much greater for thinner devices, especially if below 2um in thickness. Reduction of mask layout to the most crucial components of the device can allow for reducing the computational resources needed. Furthermore, tetrahedrons mesh can also be utilized to refine the most important regions of the device.

The analytical and simulated work illustrate the design of a new MEMS actuator which integrates 2D materials to alternate between on-off states in the quest to counteract the limitations of CMOS.

References

[1] I. A. Y. Mark T. Bohr, "CMOS Scaling Trends & Beyond," *IEEE Micro, Vol: 37 Issue 6,* pp. 20-29, November/December 2017.

[2] "Center for Energy Efficient Electronics Science: Final Period 6 Annual Report," NSF, 2016.

[3] T. Simonite, "MIT Technology Review," 25 May 2011. [Online]. Available: https://www.technologyreview.com/s/424091/what-bitcoin-is-and-why-it-matters/. [Accessed 14 June 2018].

[4] L. Mearian, "COMPUTERWORLD," 31st May 2018. [Online]. Available: https://www.computerworld.com/article/3191077/security/what-is-blockchain-the-most-disruptive-tech-in-decades.html. [Accessed 18th June 2018].

[5] J. Martindale, "Digital Trends-What is a blockchain? Here's everything you need to know," 18th April 2018. [Online]. Available: https://www.digitaltrends.com/computing/what-is-a-blockchain/. [Accessed 18th June 2018].

[6] A. Peschot, C. Qian and T.-J. King Liu, "Nanoelectromechanical Switches for Low-Power Digital Computing," *Micromachines,* pp. 1046-1065, 2015.

[7] M. Horowitz, E. Alon, D. Patil, S. Naffziger, R. Kumar and K. Bernstein, "Scaling, Power, and the Future of CMOS," in *IEEE InternationalElectron Devices Meeting*, Washington D.C., 2005.

[8] N. Z. Haron and S. Hamdioui, "Why is CMOS Scaling Coming to an End?," in *IEEE Conferences* , Monastir, 2008.

[9] S. Almeida and D. Zubia, "Monolayer strain by NEMS for low power application," in *2015 Fourth Berkeley Symposium on Energy Efficient Electronic Systems (E3S)*, Berkeley, Ca, 2015.

[10] S. F. Almeida, D. Zubia, A. Vidaña and M. Martinez, "Conductance Modulation in 2D Materials by NEMS for Lower-Power Applications," in *2017 Fifth Berkeley Symposium on Energy Efficient Electronic Systems & Steep Transistors Workshop (E3S)*, Berkeley, CA, 2017.

[11] S. Manzeli, D. Ovchinnikov, D. Pasquier, O. V. Yazyev and A. Kis, "2D transition metal dichalcogenides," *Nature Reviews Materials* , pp. 1-15, 2017.

[12] A. Kis, S. Manzeli, A. Ghadimi and A. Allain, "Piezoresistivity and Strain-induced Band Gap Tuning in Atomically Thin MoS2," *Nano Letters,* pp. 5330-5335, 2015.

[13] M. Schulz, "The end of the road for silicon?," *Nature,* pp. 729-730, 1999.

[14] A. K. Geim and K. S. Novoselov, "The rise of graphene," *Nature Materials,* pp. 183-191, 2007.

[15] Editorial, "It's still all about graphene," *nature materials,* Dec. 2010.

[16] D. Jariwala, V. K. Sangwan, L. J. Lauhon, T. J. Marks and M. C. Hersam, "Emerging Device Applications for Semiconducting Two-Dimensional Transition Metal Dichalcogenides," *ACS Nano,* pp. 1102-1120, 2014.

[17] P. Table, "Study.com," [Online]. Available: https://study.com/academy/lesson/periodic-table-for-reference.html.

[18] S. Bertolazzi, J. Brivio and A. Kis, "Stretching and Breaking of Ultrathin MoS2," *ACS Nano,* pp. 9703-9709, 2011.

[19] W. Choi, N. Choudhary, G. Hee Han , J. Park, D. Akinwande and Y. Hee Lee, "Recent development of two-dimensional transition metal dichalcogenides and their applications," *materialstoday,* pp. 116-130, 2017.

[20] K. S. Novolselov, D. Jiang, T. Booth, V. V. Khotkevich, S. M. Morozov and A. K. Geim, "Two Dimensional Atomic Crystals," *arxiv,* pp. 1-4, 2005.

[21] K. Golasa, M. Grzeszczyk, K. P. Korona, R. Bozek, J. Binder, J. Szczytko, A. Wysmolek and A. Babinski, "Optical Properties of Molybdenum Disul□de (MoS2)," in *42th □Jaszowiec□ International School and Conference on the Physics of Semiconductors*, Wisaa , 2013.

[22] K. Gołasa, M. Grzeszczyk, R. Bożek, P. Leszczyński, A. Wysmołek, M. Potemski and A. Babiński, "Resonant Raman scattering in MoS2-From bulk to monolayer," *Solid State Communications,* vol. 197, pp. 53-56, 2014.

[23] S. H. Lavington, "Early British Computers: The Story of Vintage Computers... (Book)," [Online]. Available: https://books.google.com/books?id=AU28AAAAIAAJ&pg=PA13&dq=relays+in+early+computers&hl=en&sa=X&ved=0ahUKEwjh0szXsNbaAhVDCKwKHZfqCnoQ6AEILzAB#v=onepage&q=relays%20in%20early%20computers&f=false.

[24] C. 10.0, "Using Coventorware," Coventor.

[25] G. Campardo, F. Tiziani and M. Iaculo, "Electrostatic Comb Drives," in *Memory Mass Storage*, Springer, 2011, pp. 122-123.

[26] J. J. Allen, Micro Electro Mechanical System Design, CRC Press, 2005.

[27] D. Elata and V. Leus, "How slender can comb-drive fingers be?," *IOPScience Journal of Micromechanics and Microengineering,* vol. 15, no. 5, pp. 1055-1059, 2005.

[28] A. A. A. B. Y. M. W. WAI-CHI, "Formulation of stiffness constant and effective mass for a folded beam," *Archives of Mechanics,* vol. 62, no. 5, pp. 405-418, 2010.

[29] R. W. Johnstone and A. Parmaswaran, "Ch. 10 Mechanical Components," in *An Introduction to Surface-Micromachining*, Springer, 2004.

[30] F. Cerini, M. Ferrari, V. Ferrari, A. Russo, M. Azpeitia Urquia, R. Ardito, B. De Masi and R. Sedmik, "Electro-mechanical modelling and experimental characterization of a high-aspect-ratio electrostatic-capacitive MEMS device," *Sensors and Actuators A: Physical,* vol. 266, pp. 219-231, 2017.

[31] R. Legtenberg, A. W. Groeneveld and M. Elwenspoek, "Comb-drive actuators for large displacements," *IOPSCIENCE Journal of Micromechanics and Microengineering,* vol. 6, pp. 320-329, 1996.

[32] G. Moore, "Progress in Digital Integrated Electronics," *IEEE, Int'l Electronic Devices Meeting Technical Digest,* pp. 11-13, 1975.

[33] N. S. Kim, T. Austin, D. Blaauw, T. Mudge, K. Flautner, J. S. Hu, M. J. Irwin, M. Kandemir and V. Narayanan, "Leakage Current: Moore's Law Meets Static Power," *IEEE Journals and Magazines,* pp. 68-75, 2003.

[34] C. C. Hu, Modern Semiconductor Devices for Integrated Circuits, Prentice Hall, 2010.

[35] R. Gonzalez, B. M. Gordon and M. A. Horowitz, "Supply and Threshold Voltage Scaling for Low Power CMOS," *IEEE Journal of Solid-State Circuits, Vol. 32, No. 8 ,* pp. 1210-1216, August 1997.

[36] M. Spencer, F. Chen, C. C. Wang, R. Nathanael, H. Fariborzi, A. Gupta, H. Kam, V. Pott, J. Jeon, T.-J. King Liu, D. Markovic, E. Alon and V. Stojanovic, "Demonstration of Integrated Micro-Electro-Mechanical Relay Circuits for VLSI Applications," *IEEE Journal of Solid-State Circuits (Volume: 46, Issue: 1),* pp. 308-320, Jan. 2011.

[37] J. L. Munoz-Gamarra, C. Poulain, W. Ludurczak, S. Hentz and L. Hutin, "NEMS Switches for Ultra-Low-Power Digital Logic: Challenges and Opportunities," in *2016 IEEE 16th International Conference on Nanotechnology (IEEE-NANO)*, Sendai, Japan, 2016.

[38] O. Buchnev, N. Podoliak, T. Frank, M. Kaczmarek, L. Jiang and V. A. Fedotov, "Controlling Stiction in Nano-Electro- Mechanical Systems Using Liquid Crystals," *ACS Nano,* pp. 11519-11524, 2016.

[39] A. K. Geim and I. V. Grigorieva, "Van der Waals heterostructures," *nature,* pp. 419-425, 2013.

[40] "El-CAT Inc.," [Online]. Available: https://www.el-cat.com/silicon-properties.htm. [Accessed 3 July 2018].

[41] S. A. Bhave, B. L. Bircumshaw, W. Z. Low, Y.-S. Kim, A. P. Pisano, T. J. King and R. T. Howe, "POLY-SIGE: A HIGH-Q STRUCTURAL MATERIAL FOR INTEGRATED RF MEMS," in *Solid-State Sensor, Actuator and Microsystems Workshop*, Hilton Head Island, South Carolina, 2002.

[42] J. D. Grade, H. Jerman and T. W. Kenny, "Design of Large Deflection Electrostatic Actuators," *Journal of Microelectromechanical Systems,* vol. 12, no. 3, pp. 335 - 343, 2001.

[43] Y.-C. Chen, I. C.-M. Chang, R. Chen and M. T.-K. Hou, "On the side instability of comb-fingers in MEMS electrostatic devices," *Sensors and Actuators A: Physical,* vol. 148, no. 1, pp. 201-210, 2008.

[44] C. 10.0, "Field Solver Reference," Coventor.

Vita

Mariana Martinez earned her Bachelor's in Electrical and Computer Engineering from UTEP in 2016. In the Spring of 2017 she initiated her Master's degree in the ECE department at UTEP. Her research is focused on energy efficient mechanical (MEMS) switches. During her Bachelor's and Master's she worked for the E3S center, which allowed for close collaboration with other institutions, such as UC Berkeley.

Email address: mmartinez63@miners.utep.edu

This thesis was typed by Mariana Martinez